Imperial College London

MSc QFFF Dissertation

Imperial College London

Department of Physics

Effective theory of black hole dynamics in the large D limit

Author:

Jordi Rafecas Ventosa

Supervisor:

Prof. Toby Wiseman

September 25, 2020

Submitted in partial fulfilment of the requirements for the degree of Master of Science of Imperial College London

Abstract

We begin by exploring black hole type solutions to vacuum Einstein equations in higher dimensions and we study the implications of the large D limit, i.e. assuming the number of space dimensions is infinitely large. We study the metric fluctuations of these solutions, their stability and how the perturbations classify in the large D limit. We then expand the metric tensor in powers of $1/D$ and we solve Einstein equations up to its first higher order to obtain effective theories that describe linear and non linear dynamics of black holes in the large D limit. Numerical solving of the effective equations provides us with important results regarding black hole collisions, violation of Cosmic Censorship and the evolution of Gregory-Laflamme unstable black strings. We see that the final outcome of two black hole collisions depends only on the initial angular momentum per unit mass, giving a final outcome of either a single black hole, a black bar or more the one black hole violating Cosmic Censorship in the process. We also obtain that compactified black strings evolve into a stable non uniform configuration for some values of its length, despite having an initial uniform state with an infinitesimal perturbation. We've been able to reproduce these results from the effective equations in our own numerical calculations to confirm the conclusions that are already in the literature.

Acknowledgements

I would like to express my most sincere gratitude to Prof. Toby Wiseman for giving me the opportunity to develop this Dissertation under his supervision. His dedicated help, advice, perspective and corrections have been decisive for the improvement of both the outcome of the project and my personal knowledge in physics and the world of research.

I would also like to deeply thank Prof. Roberto Emparan from Institut de Ciències del Cosmos (Universitat de Barcelona) for his help, suggestions and discussions about the topic of this project. His contribution has also been crucial to the project and the field in general. I would also like to thank Prof. Ryotaku Suzuki from Osaka City University for his attention and dedication on answering my doubts about his work.

Finally, I have to thank my family: father, mother, sister and goddaughter. Beyond financial support, each of them has been a sufficient reason for always keeping moving forward during these weird and sometimes harsh days. I wouldn't have made it to be here without them.

Contents

Chapter 1

Introduction

1.1 The ingredient: black holes in higher D

This Dissertation will exclusively deal with classical gravity in the vacuum. And yet, thousands more dissertations could be done without any need of quantising magnitudes or adding matter. Even then, classical gravity wouldn't be completed yet because the field is still fully present in current research. That's the vast power of Einstein Gravitation or General Relativity, arguably one of the finest achievements in physics of all time.

One of the most thrilling phenomena that arises from the theory is the existence of black holes. In classical gravity, spacetime is postulated to have four dimensions. Enormously powerful theorems have been proven in this case: according to the uniqueness theorem[1], in $D = 4$ all stationary axisymmetric black hole solutions of both Einstein in vacuum and Einstein-Maxwell (gravity coupled with electromagnetism) that satisfy regular boundary conditions at the horizon and asymptotically flat structure at infinity must be a member of the Kerr-Newman family of solutions, dependent only on four parameters correspondent to physical mass M, angular momentum J and electric and magnetic charges Q, P. Other deep conjectures such as Cosmic Censorship, which in short forbids the existence of naked singularities in $D = 4$[2], seem to be fully satisfied.

What happens, though, if we try to investigate the problem in higher dimensions? Fortunately, we are not the first (nor the last) to do it. Indeed, black holes in arbitrary D becomes much more difficult and hostile: none of the previous theorems and conjectures seem to prevail, and the spectrum of solutions enhances greatly as we'll see later on. Nevertheless, extra care will have to be taken regarding which of those solutions are stable (hence physically possible): many instabilities, most notably the Gregory-Laflamme instability, have been found for some of the higher D geometries.

Motivations for getting into the field are important and diverse. On one hand[3], string theories for quantum gravity are postulated in dimension $D > 4$. Closely related, AdS-CFT correspondence is built over relations between a D dimensional black hole and a $D-1$ quantum field theory[4]. Besides these two main applications, the intrinsic interest of the field seems to be already motivating enough. Black holes in higher D is, so, a fully and rich active area of research nowadays.

1.2 The tool: the large D limit

In $D = 4$, the study of black hole dynamics such as fluctuations or interactions is already impossible to evaluate analytically due to the vast non linearity of General Relativity. It comes as no surprise, then, that in the more complicated case of black holes in higher D analytical results will be close to non existent without any other assumption.

This is the reason behind why the large D limit was first suggested. Under this assumption of letting the number of space dimensions to be infinitely large, many drastic simplifications are achieved[5, 6]. Most importantly, all the gravitational effects of a mass distribution get localised on thin layer which width decreases as $1/D$ in the limit $D \to \infty$. In other words, all spacetime outside the matter content and its surrounding thin layer will be flat.

Some of its consequences are extreme. As examples, in the limit, collisions between two black holes will preserve both total entropy, hence they'll be reversible, and total energy, hence gravitational radiation will not exist.

1.3 The objective: an effective theory

As the title suggests, the final goal of this Dissertation is the construction of an effective theory so that, in the large D limit, it is capable to describe the dynamics of black holes beyond linear perturbations in a sufficiently simplified formalism that encapsulates within itself all the complexity of the problem.

Indeed, we will see that astonishingly short and simplified *effective equations* in terms of appropriate *effective variables*, very straightforward to treat numerically in contrast with many numerical GR problems, are able to evaluate non linear dynamics of large D black holes in its near region around the horizon.

Summarized, the effective equations emerge after solving vacuum Einstein equations on an appropriate metric ansatz at leading order in $1/D$ and up to its first higher order, so that non linear effects are taken in consideration. One of the main difficulties will be the construction of the initial ansatz, especially the choice of a good coordinate chart with the correct dependence on D in order to study the non linear dynamics.

1.4 The outcome: this project

Here we briefly describe the structure of this Dissertation and the basic topics one can find in each part:

- In chapter 2 we define and describe the large D limit of vacuum General Relativity and we explain its deep implications on, by simplicity, the Schwarzschild-Tangherlini black hole metric, a straightforward generalization of Schwarzschild black hole for $D = 4$. We then move forward to describe Myers-Perry metrics, which describe a rotating black hole in higher dimensions, its parameters and basic properties (horizons and singularities), and we finish their discussion by applying the large D limit on them. Next, we introduce and discuss the notion of *black branes*, a solution without any analogous at $D = 4$ where additional flat degrees of freedom are added to known black hole solutions. Finally, we very briefly describe how static black holes generalize to higher D with the presence of non vanishing electric charge or a negative cosmological constant (making the background geometry Anti de Sitter instead of flat); we also talk about other possible asymptotic topologies, the concept behind the black ring solutions.

- In chapter 3 we explain how linear black hole perturbations in arbitrary D are described in terms of *quasinormal modes*: what they are, their mathematical treatment and structure, the building of master variables and master equations that simplify and give them an intuitive meaning and the classification they follow once we assume the large D limit. We end up the section by following the calculation of the quasinormal modes, in concrete their frequencies, in the simplest case of Schwarzschild-Tangherlini black holes in the large D limit. Finally, in the last section we introduce the Gregory-Laflamme instability, which states that black branes solutions are unstable at $D \geq 5$; we follow the original mathematical derivation and the thermodynamical justification that comes along with it[7].

- In chapter 4 we move forward to introduce the concept of an effective theory: what it is, its usefulness and the key concepts from which it can be built to study black hole dynamics under the large D limit assumption. We then move to the mathematical derivation of the two effective theories that exist in the large D limit: the membrane theory and the effective theory for black branes.

We give some physical intuition to the final effective equations and effective variables of both theories.

- In chapter 5 we describe some of the main applications of the effective theory of black branes: how concrete solutions can be interpreted as Myers-Perry black holes in the large D limit and other possible solutions to the effective equations. Thanks to this correspondence, we then use the effective theory to numerically study phenomena such as collisions between black holes, violation of Cosmic Censorship and the evolution of the Gregory-Laflamme instability in black strings. Since the effective equations are reasonably easy to solve numerically, we have developed a code in Mathematica to solve them by ourselves and compare our results to those from published papers and verify them.

As a quick remark on notation, this Dissertation will always use the natural units $c = \hbar = k_B = 1$ and the East Coast or mostly positive convention $(-, +, ..., +)$ for Lorentzian metric signatures. The Newtonian constant G will be omitted in some results, always after explicit indications.

Chapter 2

Black holes in higher dimensions

2.1 The large D limit of gravity

According to General Relativity, spacetime is described as a $D = 4$ Lorentzian manifold (M, g) with Levi-Civita connection and the condition given by Einstein equations

$$R_{\mu\nu} = 0 \tag{2.1}$$

as long as there's no matter content. Obviously, this apparently short and simple equation is highly non linear, impossible to solve in general and with only a few analytical solutions, all of them after making considerable assumptions on the symmetries of the geometry.

Furthermore, in many other physical theories the equation of motion itself contains parameters: masses, coupling constants... Their presence allows us to simplify the equations by making assumptions on the parameter values that give rise to approximate solutions of the theory thanks to perturbative expansions. It's not the case of 2.1, since it lacks in any explicit parameter.

However, a natural parameter arises by considering the number of spacetime dimensions D to be arbitrary, eventually very large $D \to \infty$. We may then use the

quantity $1/D$ as an infinitesimal parameter for our theory and work analytically at leading order in its power expansion.[5, 6] This is the key idea behind the large D limit of General Relativity.

Ironically, arguably the most drastic simplification of the large D limit can already be discussed in Newtonian gravitation, which satisfies

$$\nabla^2\Phi \propto G\rho \tag{2.2}$$

For a single point mass or outside a spherically symmetric mass distribution, the solution of 2.2 is

$$\Phi \propto -\frac{1}{r^{D-2}} \Rightarrow \mathbf{g} = -\mathbf{d}\Phi \propto -\frac{D-2}{r^{D-1}}\partial_r \tag{2.3}$$

being r the Euclidean distance to the center of mass and D the number of space dimensions, excluding time. We immediately see that increasing the number of dimensions D will make both the Newtonian potential and the gravitational field to decrease faster and more abruptly outside the mass distribution.

Hence, gravitational effects will become extremely localised around massive objects: in the $D \to \infty$ limit, there will be no gravitational interaction between massive objects as long as they don't collide.

2.2 Schwarzschild-Tangherlini black holes

We study now how the large D limit simplifies black hole solutions. For this aim we start by introducing the simplest higher D black hole solution of 2.1: the Schwarzschild-Tangherlini metric [8]

$$ds^2 = -f(r)dt^2 + \frac{dr^2}{f(r)} + r^2 d\Omega_{n+1} \tag{2.4}$$

with $f(r) = 1 - (\frac{r_0}{r})^n$, $n = D-3$. Being a generalization of the Schwarzschild metric [9] for an arbitrary dimensionality, the horizon of the black hole still lies at $r = r_0$. We are going to discuss the large D limit of this solution assuming r_0 is fixed and independent of D. The main feature of 2.4 is that its metric components g_{tt} and

g_{rr} directly depend on the dimensionality in the same way the Newtonian potential does, not a coincidence given than 2.2 is the non relativistic limit of 2.4 outside a $SO(D-1)$ symmetric mass distribution.

As long as we consider D to be fixed and finite, the solution has only one characteristic length, given by the horizon r_0, which will be the length scale of all the highly non linear black hole dynamics. It is only when we allow ourselves to modify the dimensionality that a new length scale emerges. As in [5], we may evaluate the gravitational acceleration in an outside neighbourhood of the horizon:

$$\mathbf{g}|_{r0} = -\mathbf{d}\Phi|_{r0} \approx \frac{D}{r_0} \tag{2.5}$$

when $D >> 1$. Since in natural units $c = 1$ acceleration has dimensions of inverse length, we may infer that gravitational interactions outside the horizon are governed by the length scale $\frac{r_0}{D}$ i.e. objects with coordinate position r such that

$$r - r_0 >> \frac{r_0}{D} \tag{2.6}$$

will perceive no gravitational pull: spacetime will be flat wherever 2.6 holds. In the limit $D \to \infty$, all spacetime outside the horizon will be entirely flat, and the horizon will have infinite curvature. [6]

2.2.1 Small horizon

The area of a unit $D-2$ sphere S^{D-2} is

$$\Omega_{D-2} = \frac{2\pi^{\frac{D-1}{2}}}{\Gamma(\frac{D-1}{2})} \tag{2.7}$$

Since the gamma function can be approximated as $\Gamma(x) \to \sqrt{\frac{2\pi}{x}}(\frac{x}{e})^x$ for $x \to \infty$, the Stirling approximation, then the unit sphere simplifies in the large D limit into

$$\Omega_{D-2} \sim D\left(\frac{2\pi e}{D}\right)^{D/2} \to 0 \tag{2.8}$$

As consequence, keeping the r_0 fixed, the horizon of a black hole becomes infinitely small in the large D limit, since its area will be $A = r_0^{D-2}\Omega_{D-2}$, a magnitude which provides us with another characteristic length scale: the area length

$$\ell_A \equiv A^{1/(D-2)} \sim r_0 D^{\frac{1-D/2}{D-2}} \to \frac{r_0}{\sqrt{D}} \tag{2.9}$$

2.2.2 Curvature and surface gravity

From the Schwarschild-Tangherlini metric one may compute several magnitudes for all D and evaluate their behaviour in the large D limit. The value of the surface gravity is [6]

$$\kappa = \frac{D-3}{r_0} \to \infty \tag{2.10}$$

and its divergent behaviour in the large D limit is coherent with the gravitational pull on the horizon at $D \to \infty$, being both governed by the length scale $\kappa^1 = \frac{r_0}{D}$. This length scale also characterises the intrinsic curvature of the black hole; we may check it by evaluating Kretschmann scalar for the Schwarzschild-Tangherlini metric [6]

$$K = R^{\mu\nu\rho\sigma}R_{\mu\nu\rho\sigma} = \frac{(D-1)(D-2)^2(D-3)}{r^4}\left(\frac{r_0}{r}\right)^{2(D-3)} \to \left(\frac{D}{r_0}\right)^4 = \kappa^4 \tag{2.11}$$

on the horizon $r \to r_0$ for $D \to \infty$. Hence, the characteristic curvature radius of the horizon at large D decreases with the same characteristic length scale as the surface gravity and the sphere of influence: $\frac{r_0}{D}$.

2.2.3 Mass and gravitational constant

Since we will be always working in vacuum gravity, as 2.1, the gravitational constant does not appear in the fundamental equation. As it appears on the right hand side of the full Einstein equations (or in its Newtonian limit, in the source of Poisson's law), for $D = 4$ its value has been measured from experiments involving matter. In our large D treatment of gravity, the absence of G leads to some ambiguities:

- The constant G itself is ill defined, since we can't assume it has the same value as $D = 4$ for any dimensionality, simply because the dimension of G depends directly on D: from 2.3 we have

  $$[G] = L^{D-1}T^{-2}M^{-1} =_{c=1} L^{D-3}M^{-1} \tag{2.12}$$

  so the value of G should be measured for each D in experiments involving matter content, something beyond our discussion.

- Vacuum equations 2.1 are purely geometrical, so its solutions will also exclusively depend or geometrical magnitudes such as length, time and power combinations of them. In both Einstein and Newtonian gravity, geometrical quantities are related to masses only thanks to the gravitational constant G. Hence, for an arbitrary D in vacuum the ill definition of G leads to an ambiguity in quantifying masses, mainly the mass of a black hole.

- Since the physical mass of a black hole may be defined using the Newtonian limit of its metric and Einstein equations with matter, we must make the assumption that Einstein equations with matter hold for all D, including the expression its proportionality constant which carries the constant G:

$$R_{\mu\nu} - \frac{1}{2}Rg_{\mu\nu} = 8\pi G T_{\mu\nu} \quad \forall D \tag{2.13}$$

Then, the Newtonian limit of this equation may be computed [10] assuming a coordinate system for which the center of mass is fixed at the origin, $g_{\mu\nu} = \eta_{\mu\nu} + h_{\mu\nu}$ and

$$M = \int d^{D-1}xT^{00} \tag{2.14}$$

in terms of an integral over all spacelike coordinates. Its evaluation for the metric in 2.4 gives us a relation between the mass of the black hole and its horizon radius:

$$GM = \frac{(D-2)\Omega_{D-2}}{16\pi} r_0^{D-3} \tag{2.15}$$

which reduces to $2GM = r_0$ for $D = 4$, the known Schwarzschild radius expression. As a recall, this result arises after assuming 2.13 holds for any D. Its relevance lies on the dependence between the mass of the black hole and its horizon length, $M \propto \Omega_{D-2} r_0^{D-3}$, independent of our choice for the constant. In the large D limit, for fixed r_0, the smallness of the horizon leads to $GM \to 0$.

2.2.4 Absence of interactions

As stated previously, in the large D limit spacetime outside a thin neighbourhood of the horizon i.e. satisfying 2.6 is flat, so there's not gravitational attraction between massive objects. This has a direct implication on the Hawking entropy variation for

a mixing of two black holes. Using natural units $G = 1$, the Bekenstein-Hawking entropy is defined as

$$S = \frac{1}{4}A \tag{2.16}$$

being A the area of the event horizon in squared Planck length units. The Planck length depends on D

$$\ell_P = \left(\frac{\hbar G}{c^3}\right)^{\frac{1}{D-2}} \tag{2.17}$$

because of the D dependence of the dimension of G. Hence, absolute values of entropy are also ill defined, but we may still evaluate its dependence on other magnitudes. From 2.15, we can express the entropy of a black hole in terms of its mass; using again $G = 1$:

$$S(M) = \frac{1}{4}\Omega_{D-2} r_0^{D-2} = \frac{1}{4\Omega_{D-2}^{\frac{1}{D-3}}}\left(\frac{16\pi M}{D-2}\right)^{\frac{D-2}{D-3}} \sim M^{\frac{D-2}{D-3}} \tag{2.18}$$

which becomes linear with M in the large D limit, with direct consequences. Consider an initial set of n_i Schwarzschild-Tangherlini black holes with masses M_j, $M_i = \sum_j^{n_i} M_j$, that interact and evolve into a final state of n_f black holes with masses M'_j, $M_f = \sum_j^{n_f} M'_j$. According to black hole mechanics, a possible defect of mass may be emitted via gravitational radiation, so $M_f \leq M_i$. However, the second law implies $dS \geq 0$. At finite D, it is possible to recombine several black holes in an irreversible process with emission of gravitational waves. However, in the large D limit we have $S \propto M$, which implies

$$dS \geq 0 \Rightarrow M_f \geq M_i$$
$$dM \leq 0 \Rightarrow M_f \leq M_i$$

with unique solution for $M_f = M_i$. In conclusion, in the large D limit, black hole merging or splitting will never emit gravitational radiation, entropy will never be gained so the process will be always reversible and the total mass will be conserved. We can interpret this important result as a consequence of the absence of interactions between the black holes in the large D limit; a consequence of spacetime being flat outside their event horizons.

2.3 Myers-Perry black hole

As far as 2.4 is the generalization of the Schwarzschild black hole for any D, the Myers-Perry black hole generalizes the Kerr or rotating black hole to any D.

2.3.1 Flat rotation in D dimensions

Consider a Euclidean space in $D-1$ dimensions. An infinitesimal spatial rotation of the coordinates will be characterized by an antisymmetric $D-1 \times D-1$ matrix, which is the property of any element of $SO(D-1)$ Lie algebra.

From linear algebra, we know that any non singular $2n \times 2n$ antisymmetric matrix R satisfies

$$O = \Lambda^T R \Lambda \tag{2.19}$$

where $\Lambda \in SO(D-1)$ and O is a block diagonal matrix with the following shape:

$$O = \begin{pmatrix} 0 & -J_1 & ... & 0 & 0 \\ J_1 & 0 & ... & 0 & 0 \\ ... & ... & ... & ... & ... \\ 0 & 0 & ... & 0 & -J_n \\ 0 & 0 & ... & J_n & 0 \end{pmatrix} \tag{2.20}$$

being $\pm iJ_i$ the eigenvalues of R. The result holds for $2n+1 \times 2n+1$ antisymmetric matrices; then, O will have an extra row and column with only zeros. The relevance of 2.19 lies on the fact that, given a general rotation linear with time such as that of a stationary rotating black hole, we can always choose an appropriate coordinate chart for which the general rotation decomposes into several plane rotations, each affecting only a pair of coordinates and parametrised by the eigenvalues of O, which physically correspond to angular momentum.

2.3.2 Angular momentum tensor and coordinate charts

As discussed, a general rotation in $D-1$ spatial dimensions will be characterised by individual rotations over 2-planes defined by pairs of spacelike coordinates. We'll treat separately the cases where D is even or odd [10]. Starting from a flat D dimensional metric, assuming odd D,

$$ds^2 = -dt^2 + dx_i dx_i, \quad i = 1, ..., D-1$$
$$ds^2 = -dt^2 + dx_i dx_i + dy_i dy_i, \quad i = 1, ..., \frac{D-1}{2}$$

We may insert flat polar coordinates to each pair:

$$x_i = r\mu_i \cos\phi_i$$
$$y_i = r\mu_i \sin\phi_i$$

so that $r^2 = x_i x_i + y_i y_i$, i.e. $\mu_i \mu_i = 1$ [10]. The metric becomes

$$ds^2 = -dt^2 + dr^2 + r^2 \sum_{i=1}^{(D-1)/2} (d\mu_i^2 + \mu_i^2 d\phi_i^2) \tag{2.21}$$

where one of the coordinates is constrained by the others. For the case where D is even we just need to add an extra cartesian coordinate $z = r\alpha$ with $\alpha \in [-1, +1]$, adding a $r^2 d\alpha^2$ term to the flat metric in polar coordinates. Then, the constraint becomes $\mu_i \mu_i + \alpha^2 = 1$.

The metric in this chart directly shows a set of $\frac{D-2}{2}$ (even D) or $\frac{D-1}{2}$ (odd D) commuting Killing vectors, $\xi_i = \partial_{\phi_i}$. Those vectors mark the direction of each plane rotation. Each parameter will be related to angular momentum. Given the shape of 2.20, we'll define angular momentum in D dimensions as an antisymmetric 2-tensor, with $\frac{D-2}{2}$ (even D) or $\frac{D-1}{2}$ (odd D) degrees of freedom.

2.3.3 Myers-Perry metric

Using an appropriate chart for the spacelike coordinates, the metric of a Myers-Perry black hole is the following[10]:

$$ds^2 = -dt^2 + \frac{r r_0^{D-3}}{\Pi F}\left(dt + a_i \mu_i^2 d\varphi_i\right)^2 + \frac{\Pi F}{\Pi - r r_0^{D-3}} dr^2 + \left(r^2 + a_i^2\right)\left(d\mu_i^2 + \mu_i^2 d\varphi_i^2\right) + r^2 d\alpha^2 \tag{2.22}$$

$$F = 1 - \frac{a_i^2 \mu_i^2}{r^2 + a_i^2}$$

$$\Pi = \prod_{i=1}^{(D-2)/2} \left(r^2 + a_i^2\right)$$

for even D, assuming summation for $i \in 1, ..., \frac{D-2}{2}$, and

$$ds^2 = -dt^2 + \frac{r^2 r_0^{D-3}}{\Pi F}\left(dt + a_i \mu_i^2 d\varphi_i\right)^2 + \frac{\Pi F}{\Pi - r^2 r_0^{D-3}} dr^2 + \left(r^2 + a_i^2\right)\left(d\mu_i^2 + \mu_i^2 d\varphi_i^2\right) \tag{2.23}$$

for odd D, with the same expressions for Π, F and assuming summation now for $i \in 1, ..., \frac{D-1}{2}$.

As expectable, the set of parameters (a_i, r_0) encode the physical mass of the black hole and the angular momentum over each direction by examining the asymptotic behaviour in the non relativistic limit. The result for the mass is the same as that for Schwarzschild-Tangherlini, 2.15. In parallel with 2.14, we define the physical angular momentum tensor as[10]

$$J^{\mu\nu} = \int d^{D-1}x \left(x^\mu T^{0\nu} - x^\nu T^{0\mu}\right) \tag{2.24}$$

which is related to the parameters as

$$J^{y_i, x_i} = \frac{\Omega_{D-2}}{8\pi G} r_0^{D-3} a_i = \frac{2}{D-2} M a_i \tag{2.25}$$

in the current coordinate basis. All other components vanish. For all D, a_i corresponds to an angular momentum per unit mass up to a constant factor. Because of the horizon smallness property, for fixed r_0, all components of J^{ij} vanish in the large D limit.

The Myers-Perry metrics 2.22 and 2.23 have, respectively, $\frac{D}{2}$ and $\frac{D+1}{2}$ symmetries: time translation $k = \partial_t$ and all the n polar phase shifts $m_i = \partial_{\varphi_i}$; all Killing vectors commute, so the symmetry is $\Re \times U(1)^n$. Particular cases where some of the parameters a_i are zero or coincide increase the symmetries of Myers-Perry metric. Concretely, if $a_1 = a_2 = ... = a_m$, its corresponding symmetry grows from $U(1)^m$, with dimension m, to $U(m)$, dimension $m^2 \geq m$, with respect to the coordinates $z_i = \mu_i e^{i\varphi_i}$[10].

The Kerr metric is the particular case of 2.22 for $D = 4$; as in Kerr spacetime, all Myers-Perry black holes are stationary, since no metric components depend on the timelike coordinate; nevertheless they are not static, since non vanishing $g_{t\varphi_i}$ components break time reversal symmetry.

2.3.4 Singularities

Let's briefly discuss some physical features of Myers-Perry black holes. Again, we'll treat by separate the even and odd D cases.

From 2.22 and 2.23, some component of the Myers-Perry metric diverges for

$$\frac{\Pi F}{r^\gamma} = 0 \tag{2.26}$$

whose solutions lead to physical singularities [10], and

$$r^\gamma = \frac{\Pi}{r_0^{D-3}} \tag{2.27}$$

whose solutions lead to coordinate singularities on event horizons. In both equations and from now on, we use

$$\gamma = 1 + D \mod 2 \tag{2.28}$$

For even D, as long as all $a_i \neq 0$, the most general rotation, physical singularities will show a topology of S^{D-3} since they lie at $r = 0 \cap \alpha = 0$, the only solution of 2.26 and a generalization of Kerr's ring singularity, its $D = 4$ case. If some $a_i = 0$ the physical singularity arises at $r = 0$ with no further requirements.

For odd D, if all $a_i \neq 0$, there's no singularity since $\frac{\Pi F}{r^2} = 0$ remains finite for $r \to 0$, existing no solutions of 2.26 for $\gamma = 2$. If only one $a_i = 0$, say $a_1 = 0$, for $r \to 0$ then $\Pi \sim r^2$ and $F \sim \mu_1 + r^2$, so the singularity corresponds to $r = 0 \cap \mu_1 = 0$, with topology of S^{D-3}. Moreover, $r = 0$ without further restrictions corresponds to a conical singularity [10]. If more than one rotation eigenvalue vanishes, then $r = 0$ always solves 2.26 and hence always leads to a curvature singularity.

2.3.5 Horizons

Regarding the horizons, always assuming $r_0 > 0$, the horizon condition 2.27 is a polynomial equation of order $D - 3 + \gamma$, being the horizons its non zero solutions. Hence, they have no analytical expression in general. Since they are constraints only affecting r, all of them have a topology of S^{D-2}.

For even D, however, there will never be more than two horizons: studying the extremes of the horizon equation

$$P(r) = \Pi(r) - r r_0^{D-3} \tag{2.29}$$

being $P(r_H) = 0$ the condition of the horizons, we have

$$P'(r) = \Pi'(r) - r_0^{D-3} \tag{2.30}$$

$\Pi(r) \sim r^{D-2}$ for $r \to \infty$, and both $\Pi(r)$ and $\Pi'(r)$ are monotonically increasing. Hence, there's only up to one value that satisfies $P'(r) = 0$ for $r > 0$, which will correspond to a minimum of P by continuity. As consequence, no more than two solutions can emerge from $P(r) = 0$, leading to no more than two event horizons for all even values of D, just as in Kerr spacetime. If some $a_i = 0$, then one solution is always $r = 0$, already a physical singularity, leaving one and only one alternative $r > 0$ horizon, regardless of the amount of spin in the other orthogonal planes, setting a key difference with Kerr black hole, where large spin leads to a naked singularity. These cases are known as ultra-spinning black holes.[10]

For odd D, proceeding as in the previous case, horizons lie at $P(r) = 0$ being

$$P(r) = \Pi(r) - r^2 r_0^{D-3} \tag{2.31}$$

Analysing its extremes, we have

$$P'(r) = \Pi'(r) - 2r r_0^{D-3} \tag{2.32}$$

Since $\frac{\Pi'(r)}{r}$ is monotonically increasing with r^2, no more than one solution for r^2 can emerge. By continuity, we'll have either a single minimum of 2.31 at $r = 0$ and no horizons whatsoever since $\Pi(0) \geq 0$, or a maximum at $r = 0$ and minimums at $r = \pm r_* \neq 0$, allowing possible $r > 0$ horizon solutions. The condition for a maximum at $r = 0$, necessary but not sufficient for the existence of horizons, is

$$r_0^{D-3} > \sum_i \prod_{j \neq i} a_j^2 \tag{2.33}$$

If the condition holds, we may find again up to two different horizons at $r > 0$, which will have topology of S^{D-2} since they only constrain r. Note that a key behaviour is different between odd and even D: we see from 2.33 that for odd D, a single vanishing $a_i = 0$ doesn't guarantee the presence of an event horizon regardless of the value of the remaining a_j, in opposition with the already discussed ultra-spinning black holes at even D. It will be only when at least two different $a_i = 0$ vanish simultaneously that $r = 0$ will be a solution and, for $r_0 > 0$, a single event horizon at $r > 0$ is guaranteed for all values of the remaining a_j. In conclusion, for odd D, at least two different plane rotations must vanish in order to have ultra-spinning black holes.

The surface gravity has the following value[10]:

$$\kappa = \frac{\Pi'(r) - \gamma r_0^{D-3} r^{\gamma-1}}{2 r_0^{D-3} r^{\gamma}} |_{r_H} \tag{2.34}$$

still using 2.28 for the value of γ.

2.3.6 Large D limit

Consider, for simplicity, the particular case $a_1 = a_2 = ... = a_k \equiv a$, $a_{k+1} = ... = a_{(D-3+\gamma)/2} = 0$, and let $D \to \infty$ [6]. We'll have to analyse separately the cases where the number of rotating planes remains fixed, i.e. constant k, and where the number of rotating planes grows infinitely, i.e. $k \to \infty$.

From its definition, we have $\Pi(r) = r^{D-3+\gamma}\left(1+\left(\frac{a}{r}\right)^2\right)^k$. Hence, for both odd and even D the horizon equation 2.27 becomes

$$\frac{r_0}{r_H} = \left(1+\left(\frac{a}{r_H}\right)^2\right)^{k/(D-3)} \tag{2.35}$$

which in the large D limit simplifies to $r_H \to r_0$ as long as the limit is applied to the number of non rotating planes, i.e. leaving k fixed.

In the alternative case where k grows linearly with D, assume the number of non rotating planes $m = \frac{D-3+\gamma}{2} - k$ remains fixed when $D \to \infty$ [6]. Then we may rewrite the 2.35 as

$$\frac{r_0}{r_H} = \left(1+\left(\frac{a}{r_H}\right)^2\right)^{\frac{1}{2}\left(1-\frac{m-\gamma}{D-3}\right)} \tag{2.36}$$

which in the large D limit with constant m is solved by $r_H = \sqrt{r_0^2 - a^2}$.

2.4 Black branes

2.4.1 Definition

Black p-branes are solutions of vacuum Einstein equations 2.1 in higher dimensions of the form

$$ds^2 = g_{\mu\nu}dx^\mu dx^\nu = -\left(1-\left(\frac{r_0}{r}\right)^n\right)dt^2 + \frac{dr^2}{1-\left(\frac{r_0}{r}\right)^n} + r^2 d\Omega_{n+1} + \sum_{i=1}^{p} dx^{i2} \tag{2.37}$$

where $n = D - p - 3$. Intuitively, a black brane is a higher dimensional extension of the known Schwarzschild-Tangherlini black hole where the new coordinates don't increase the spherical symmetry but, instead, they add a simple extra flat dimension to spacetime.

The metric of a black brane can also be written as a covariant expression with respect to boosts along the flat directions:

$$ds^2 = \left[\eta_{ab} + \left(1-\left(\frac{r_0}{r}\right)^n\right)u_a u_b\right]dx^a dx^b + \frac{dr^2}{1-\left(\frac{r_0}{r}\right)^n} + r^2 d\Omega_{n+1} \tag{2.38}$$

where u_a is a $p+1$-velocity vector along the *worldvolume* of the brane, i.e. its free directions plus time, and a, b indices run over $t, 1, ..., p$.

Black 1-branes, i.e. $p = 1$, are also called *black strings*.

2.4.2 Stress tensor

Despite being solutions to vacuum Einstein equations, we can associate a non vanishing stress-energy tensor to a black brane by studying its asymptotic behaviour. As extensions of black holes, the stress tensor of a brane extends the notion of the mass of the black hole. The extended expression is the following[11]:

$$T_{ab} = \frac{1}{16\pi G}\int_{r\to\infty} d\Omega_{n+1} r^{D-p-2} n^i \left[\eta_{ab}\left(\partial_i h^c_c + \partial_i h^j_j - \partial_j h^j_i\right) - \partial_i h_{ab}\right] \tag{2.39}$$

where $h_{\mu\nu} = g_{\mu\nu} - \eta_{\mu\nu}$ is the asymptotic deviation from the flat metric, $a, b, c...$ run over the brane worldvolume and $i, j, ...$ run over the transverse directions (radial and angles). n^i is a unit vector on the direction of ∂_i. The following extension has been developed so that, as expected, the component 00 will return the known mass of the black hole.

The notion of a stress tensor associated to the brane gives raise to an equation of state for the brane itself. For a neutral and asymptotically flat brane like 2.37, one may calculate the energy density $\epsilon = T_{00}$ and pressure $T_{ab} = P\eta_{ab}$ and prove that they are related via the following equation of state[12]:

$$P = -\frac{\epsilon}{D-p-2} = -\frac{\epsilon}{n+1} \tag{2.40}$$

For any equation of state, one may compute the speed of sound[13]

$$v = \sqrt{\frac{dP}{d\epsilon}} = \sqrt{\frac{-1}{n+1}} \tag{2.41}$$

which is imaginary due to Gregory-Laflamme instabilities[12] as we'll see in the next chapter. In module, in the large D limit $v \sim 1/\sqrt{D} \to 0$, so the characteristic length scale of fluctuations along the worldvolume will be of order $1/\sqrt{D}$ and, thus, the latter may be studied in a non relativistic framework.

2.5 Other solutions

2.5.1 Static charged black holes

Just like the Reissner-Nordström solution easily generalises the Schwarzschild black hole when coupling gravity to static electromagnetism, in higher dimensions the Schwarzschild-Tangherlini metric can be easily extended for charged static and spherically symmetric black holes[6, 14, 15]:

$$ds^2 = -f(r)dt^2 + \frac{dr^2}{f(r)} + r^2 d\Omega_{D-2}, \quad f(r) = 1 - \left(\frac{r_0}{r}\right)^{D-3} + \left(\frac{r_Q}{r}\right)^{2(D-3)} \tag{2.42}$$

where $r_Q^{D-3} = Q\sqrt{\frac{8\pi G}{(D-2)(D-3)}}$, being Q the electromagnetic charge of the black hole.

2.5.2 Anti de Sitter black holes

Almost the entirety of this Dissertation could be discussed again assuming that the background space geometry, and so also the asymptotic topology, is Anti de Sitter (constant curvature R and constant cosmological constant $\Lambda < 0$) instead of asymptotically flat. I'll leave that for a future student. Here we will only discuss the static solution with non vanishing negative cosmological constant. Just like charged black holes, the solution quickly generalises[16]. The metric is [6]

$$ds^2 = ds^2 = -f(r)dt^2 + \frac{dr^2}{f(r)} + r^2 d\Omega_{D-2}, \quad f(r) = 1 - \left(\frac{r_0}{r}\right)^{D-3} + \frac{r^2}{L^2} \tag{2.43}$$

where $L^2 = \sqrt{\frac{(D-1)(D-2)}{2|\Lambda|}}$. L has dimensions of length, so it defines a new length scale without any analogous in asymptotically flat spaces: $L \sim D/\sqrt{|\Lambda|}$. Hence, as long as Λ remains fixed when we take the large D limit, all effects of the background curvature will disappear since $L \to \infty$, making the Anti de Sitter space flat in the limit. Hence, to study AdS spaces in the large D, Λ must diverge proportional to D^2 so that the length scale of AdS effects L remains finite.

2.5.3 Black rings

Black rings[17, 18] are solutions that, as a key property, present a different asymptotic topology than the usual flat D-dimensional Minkowski space. Their metric is

$$ds^2 = -dt^2 + \frac{R^2}{(R + r\cos\theta)^2}\left[\frac{R^2 dr^2}{R^2 - r^2} + (R^2 - r^2)d\Phi^2 + r^2(d\theta^2 + \sin^2\theta d\Omega_n)\right] \quad (2.44)$$

where $D = n + 4$ and the domain of the coordinates is $\Phi \in (0, 2\pi)$, $r \in (0, R)$, being R the radius of the ring. At constant r, the spatial topology is $S^1 \times S^{n+1}$, radically different from any of the metrics previously described.

Chapter 3

Fluctuations of black holes

3.1 Introduction

After a general review and presentation of the many different black hole solutions that exist in higher dimensions and their properties once we apply the large D limit, we aim now to explain the behaviour of black hole fluctuations, i.e. small perturbations from a known black hole metric.

Two key concepts arise from the following perturbation analysis: the fluctuations in terms of quasinormal modes and the stability of those modes, which will lead to fundamental results regarding whether some known black hole solutions are actually stable or not against small time dependent fluctuations. The most important result is what we call the Gregory-Laflamme instability, which states that certain black branes and black strings are unstable. In the further development of effective theories to describe black hole dynamics, we expect them to be able to predict both of this phenomena, which will represent a major test on the utility of the mentioned theories.

3.2 Quasinormal modes

3.2.1 Qualitative features

We call quasinormal modes (often abbreviated as QNM in the upcoming of this paper) to each of the oscillations in a characteristic time frequency in which a given metric fluctuation can be decomposed[5]. For stationary black hole configurations, the discrete or continuous set of frequencies in which one may decompose a metric fluctuation is named as the quasinormal spectrum.

The reason behind this nomenclature is intuitive: in many aspects quasinormal modes remind of a typical Fourier decomposition of a fluctuation into a linear combination of eigenfunctions, the normal modes, of a given self-adjoint differential operator (in the Fourier case, the harmonic or Laplacian operator). In our case, we're not allowed to talk about normal modes because of boundary issues: since their domain is the region outside the black hole, their boundaries are the horizon and asymptotically flat infinity. While in the latter case homogeneous boundary constraints hold, we can't state the same on the horizon[5], since the nature of the black hole will absorb part of the fluctuating energy distribution of the mode. Their dissipative properties are manifested by their frequencies becoming complex in a $\propto e^{-i\omega t}$ expression.

This lack of a homogeneous boundary condition on the horizon is also the reason behind the quasinormal spectrum doesn't form a complete basis of modes in which any fluctuation may be completely decomposed. Nevertheless, their importance remains crucial since QNM still fully describe the final stages of the fluctuation after the black hole has been perturbed before their final turn back to equilibrium.

The mathematical calculation of quasinormal modes and spectrum is far from trivial; here we will follow the relevant steps and points of the procedure but we will skip the most solely algebraic part. In summary, the final and most important

prediction is that quasinormal modes can be classified into one of two families of modes that differ from each other on how their spectrum frequencies depend on the dimensionality of spacetime in the large D limit[5, 19, 20]:

- Non decoupled modes: their defining property is that their frequencies are dependent on the dimensionality D by $\omega \sim D/r_0$ at leading order. For this reason, in the large D limit framework they are also called *fast* modes. Their location is spread, since they extend from the near region up to the asymptotic zone[20], and they carry little further information, since they are universal in all solutions of asymptotically flat black holes and their single parametric dependence is on the event horizon r_0 and D.

- Decoupled modes: their defining property is that their frequencies are independent of the dimensionality D by $\omega \sim 1/r_0$ at leading order for all values of D, being called *slow* modes by contrast in the large D limit. Contrary to the fast modes, they are strongly localized in the near region, quickly decoupling and vanishing in the far zone, hence the name of their class. There are much less that non decoupled modes, and they hide many more physically interesting features: they encode horizon instabilities and are unique for each type of black hole[5]. Effective theories mostly emphasize on trying to predict their dynamics.

3.2.2 Tensor decomposition of fluctuations

Consider a spacetime of dimension $m + n$ which is the result of a product of two manifolds of dimensions m and n, respectively. Assume that the latter is a n-dimensional Riemannian Einstein manifold with constant intrinsic curvature $K = -1, 0, +1$[21, 22, 23]. Then, the metric can be written as

$$ds^2 = g_{\mu\nu}dx^\mu dx^\nu = g_{ab}(y)dy^a dy^b + r^2(y)\gamma_{ij}dx^i dx^j \tag{3.1}$$

where y^a are coordinates on the m-manifold and x^i on the n-manifold and γ_{ij} is the metric of a constant curvature Riemannian space: either S^n, H^n or E^n. From now

on, covariant derivatives and curvature tensors labeled with Latin $(i, j, k...)$ indices will refer to these objects defined on the n-manifold, not the whole spacetime. Same for $(a, b, c...)$ indices on the m-manifold. Because of Einstein equations, the stress-energy tensor $\Theta_{\mu\nu}$ carries, as expected, an additional symmetry: $\Theta_{ia} = 0$, $\Theta^i_j = P\delta^i_j$.

In order to analyze perturbations, it is fundamental to avoid any unphysical freedom: we will be only interested in gauge invariant quantities. Consider a perturbation $h_{\mu\nu}$ from spacetime 3.1, which may carry an associated energy distribution $\delta\Theta_{\mu\nu}$ so that Einstein equations hold. Apply, then, an infinitesimal gauge transformation $x^\mu \to x^\mu + \xi^\mu$. Objects will transform proportional to Lie derivatives[21]:

$$\delta h_{\mu\nu} = -\pounds_\xi g_{\mu\nu} = -(\nabla_\mu \xi_\nu + \nabla_\nu \xi_\mu) \tag{3.2}$$

$$\delta h_{ab} = -\nabla_a \xi_b - \nabla_b \xi_a \tag{3.3}$$

$$\delta h_{ia} = -r^2 \nabla_a \left(\frac{\xi_i}{r^2}\right) - \nabla_i \xi_a \tag{3.4}$$

$$\delta h_{ij} = -\nabla_i \xi_j - \nabla_j \xi_i - 2r\gamma_{ij}\xi^a \nabla_a r \tag{3.5}$$

$$\delta(\delta\Theta_{\mu\nu}) = -\pounds_\xi \Theta_{\mu\nu} \tag{3.6}$$

$$\delta(\delta\Theta_{ab}) = \xi^c \nabla_c \Theta_{ab} - \Theta_{ac}\nabla_b \xi^c - \Theta_{bc}\nabla_a \xi^c \tag{3.7}$$

$$\delta(\delta\Theta_{ia}) = -\Theta_{ab}\nabla_i \xi^b - r^2 P \nabla_a \left(\frac{\xi_i}{r^2}\right) \tag{3.8}$$

$$\delta(\delta\Theta_{ij}) = -\gamma_{ij}\xi^a \nabla_a (Pr^2) - P(\nabla_i \xi_j + \nabla_j \xi_i) \tag{3.9}$$

We've specified separately the (ab), (ai) and (ij) expressions, only in terms of tensor objects on the original manifolds because we will decompose the fluctuation in its scalar, vector, and 2-tensor part according to its transformation properties on the constant curvature n-manifold. Each of these three sectors will have their own set of eigenfunctions and eigenvalues. Regarding notation, we'll repeatedly use $\Delta = \nabla^i \nabla_i$, the Laplacian on the n-manifold.

First, we need to state the defining equation and properties of eigenscalars, vectors and tensors.[21] Then, we need to find all the possible ways they can appear in the metric and stress tensor fluctuations, and finally keep only quantities that remain gauge invariant according to 3.2, 3.6. Applying Einstein equations to these gauge

invariant quantities will give us the equations of motion for the fluctuations.[22, 23] Throughout the whole section we'll assume vanishing cosmological constant $\Lambda = 0$.

Tensor sector

The tensor eigenfunctions of the harmonic operator must obey[21]

$$(\Delta + k^2)T_{ij} = 0, \quad T_i^i = \nabla_j T_i^j = 0 \tag{3.10}$$

The first equation is the expected definition of the eigenfunction, while extra properties are required because non traceless or non vanishing divergence tensors will emerge from other sectors. The Laplace operator with a boundary condition has only positive eigenvalues, with the addition of $k = 0$ (constant tensors) only if the space is flat $K = 0$[21]. The spectrum is continuous for $K \leq 0$ and discrete for $K = +1$, with eigenvalues[22]

$$k^2 = \ell(\ell + n - 1) - 2; \quad \ell = 1, 2, ... \tag{3.11}$$

Since no contraction is allowed by construction, only tensor components of the metric and stress tensor can be built from eigenfunctions of the tensor sector. Hence,

$$h_{ab} = h_{ai} = 0, \quad h_{ij} = 2r^2 H_T T_{ij} \tag{3.12}$$

$$\delta\Theta_{ab} = \delta\Theta_{ai} = 0, \quad \delta\Theta_{ij} = \tau_T T_{ij} \tag{3.13}$$

where summation over all eigenvalues is assumed. Since the gauge transformation vector ξ^μ can't be built from any eigentensor combination, functions H_T and τ_T are directly gauge invariant and can be present in the motion equations[21]. One may calculate the perturbed Ricci tensor $\delta R_{\mu\nu}$ resulting from the fluctuation $h_{\mu\nu}$. Then, Einstein equations require

$$-\nabla^a\nabla_a H_T - \frac{n}{r}\nabla^a r \nabla_a H_T + \frac{k^2 + 2K}{r^2} H_T = 8\pi\tau_T \tag{3.14}$$

which is the only perturbation equation for the tensor sector[21].

Vector sector

The vector eigenfunctions of the harmonic operator must obey

$$(\Delta + k^2)V_i = 0, \quad \nabla_i V^i = 0 \tag{3.15}$$

where, again, the extra vanishing divergence property is due to non divergent vectors being part of the scalar sector, as we will see later. Linked to the vector eigenfunctions we can define a new tensor quantity,

$$V_{ij} = -\frac{1}{k}\nabla_{(i}V_{j)} \tag{3.16}$$

which is traceless but not divergence free, as opposed to the tensors from the tensor sector. From 3.15 and 3.16 we can write

$$[\Delta + k^2 - (n+1)K]V_{ij} = 0, \quad \nabla_j V_i^j = \frac{k^2-(n-1)K}{2k}V_i \tag{3.17}$$

which is a harmonic equation too. Hence, tensors that are traceless but not divergence free can be built from eigenfunctions V_{ij} that, despite being 2-tensors, arise from the vector sector of the decomposition. Again, boundary conditions on 3.15 guarantees $k^2 \geq 0$, with only $k = 0$ for a constant vector if space is flat. The spectrum, again, is only quantised if $K = +1$, with eigenvalues

$$k^2 = \ell(\ell+n-1) - 1; \quad \ell = 1, 2, ... \tag{3.18}$$

Note, though, that $k^2 > 0$ still doesn't ensure positiveness on the eigenvalues of V_{ij} in 3.17. When this happens, i.e. $0 < k^2 < (n+1)K$, 3.17 can only hold if, trivially, $V_{ij} = 0$ and, thus, V_i is a Killing vector by construction, with eigenvalue $k^2 = (n-1)$ as long as $K = +1$, so that the divergence condition in 3.17 holds.

Repeating the procedure from 3.12 and 3.13, let's express $h_{\mu\nu}$ and $\delta\Theta_{\mu\nu}$ in terms of the eigenfunctions from the vector sector:

$$h_{ab} = 0, \quad h_{ai} = r f_a V_i, \quad h_{ij} = 2r^2 H_T V_{ij} \tag{3.19}$$

$$\delta\Theta_{ab} = 0, \quad \delta\Theta_{ai} = r\tau^a V_i, \quad \delta\Theta_{ij} = \tau_T V_{ij} \tag{3.20}$$

As a reminder, summation over all the spectrum is assumed. Now, a gauge transformation can be built with eigenfunctions from the vector sector, by setting $\xi_a = 0$, $\xi_i = rLV_i$, where $L = L(y^a)$. Substituting in 3.2 equations, we evaluate the gauge transformation behaviour of τ^a, f_a, H_T and τ_T. τ_T and τ^a are directly gauge invariant. The other two are not, but the linear combination $F_a = f_a + \frac{r}{k}\nabla_a H_T$ is[21]. For the special case of the mode with eigenvalue $k^2 = (n-1)K > 0$, in which V_{ij} vanishes, H_T and τ_T are not defined, and only the combination $F_{ab} = 2r\nabla_{[a}\frac{f_{b]}}{r}$ is gauge invariant.

Finally, the requirement of Einstein equations gives us the perturbation equations for the vector sector:

$$\frac{2}{r^{n+1}}\nabla^b\left(r^{n+2}\nabla_{[b}\frac{F_{a]}}{r}\right)-\frac{k^2-(n-1)K}{r^2}F_a=-16\pi\tau_a \quad if \quad k^2\neq(n-1)K \tag{3.21}$$

$$\frac{k}{r^n}\nabla_a(r^{n-1}F^a)=-8\pi\tau_T \quad if \quad k^2\neq(n-1)K \tag{3.22}$$

$$\frac{1}{r^{n+1}}\nabla^b(r^{n+1}F_{ab})=-16\pi\tau_a \quad if \quad k^2=(n-1)K \tag{3.23}$$

These equations fully describe the vector sector of metric perturbations in terms of up to three gauge invariant variables: F_{ab} or τ_a, τ_T and F_a.

Scalar sector

The scalar eigenfunctions of the harmonic operator must obey

$$(\Delta+k^2)S=0 \tag{3.24}$$

from which we can build a vector

$$S_i=-\frac{1}{k}\nabla_i S\Rightarrow\nabla_i S^i=kS,\quad(\Delta+k^2-(n-1)K)S_i=0 \tag{3.25}$$

and a tensor too,

$$S_{ij}=\frac{1}{k^2}\nabla_i\nabla_j S+\frac{1}{n}\gamma_{ij}S\Rightarrow\nabla_j S_i^j=\frac{n-1}{n}\frac{k^2-nK}{k}S_i,\quad(\Delta+k^2-2nK)S_{ij}=0 \tag{3.26}$$

which is still traceless but again not divergence free. Both S_i and S_{ij} are eigenfunctions of the harmonic operator. Now $k=0$ is in the spectrum for all $K\geq 0$ (for $K<0$ it's not normalizable)[21], corresponding to a constant function, while in the vector and tensor sectors that happened only for $K=0$. Note that for $k=0$ both S_i and S_{ij} don't exist. Aside from that, boundary conditions in both 3.25 and 3.24 require $k^2>(n-1)K>0$. $S_i=0$ carries a degeneracy since it only requires S to be constant. The spectrum only quantises for $K=+1$ and its eigenvalues are

$$k^2=\ell(\ell+n-1);\quad \ell=0,1,2,... \tag{3.27}$$

The scalar section is the longest and most tedious to develop, since all metric and stress tensor components of the fluctuation contribute[21]:

$$h_{ab}=f_{ab}S,\quad h_{ai}=rf_aS_i,\quad h_{ij}=2r^2(H_TS_{ij}+H_L\gamma_{ij}S) \tag{3.28}$$

$$\delta\Theta_{ab}=\tau_{ab}S,\quad \delta\Theta_{ai}=r\tau^aS_i,\quad \delta\Theta_{ij}=(\tau_TS_{ij}+\delta P\gamma_{ij}S) \tag{3.29}$$

in terms of 8 objects: f_{ab}, f_a, H_T, H_L, τ_{ab}, τ^a, τ_T and δP. Here's why we had assumed all our tensors from the three sectors to be traceless: we impose that all the perturbations on the trace are controlled by functions H_L, δP that multiply the original metric tensor on the Einstein manifold γ_{ij}, so that the behaviour on the trace is clearly separated from the "shear" fluctuation. Note that no S_iS_j term appears (neither does V_iV_j in the vector sector) because we are working with only linear combinations of our constituents.

A gauge transformation can now be expressed as $\xi_a = T_aS$, $\xi_i = rLS_i$. Substituting the metric and stress tensor expressions back in 3.2 equations, we find the gauge transformation properties of all our objects. From all, only τ_T is directly gauge invariant. Using $X_a = \frac{r}{k}\Big(f_a + \frac{r}{k}\nabla_a H_T\Big)$, 5 more gauge invariant quantities may be built[21]:

$$F = H_L + \frac{1}{n}H_T + \frac{1}{r}X^a\nabla_a r \tag{3.30}$$

$$F_{ab} = f_{ab} + 2\nabla_{(a}X_{b)} \tag{3.31}$$

$$\Sigma_{ab} = \tau_{ab} + 2\Theta^c_{(a}\nabla_{b)}X_c + X^c\nabla_c\Theta_{ab} \tag{3.32}$$

$$\Sigma_a = \tau_a - \frac{k}{r}(\Theta^b_a X_b - PX_a) \tag{3.33}$$

$$\Sigma = \delta P + X^a\nabla_a P \tag{3.34}$$

and, as function of these quantities, Einstein equations lead to the following vastly long motion equations for perturbations in the scalar sector[21]. Using $\Box = \nabla^a\nabla_a$:

$$\begin{aligned}
&-\Box F_{ab} + \nabla_a\nabla_c F^c_b + \nabla_b\nabla_c F^c_a + \frac{n}{r}\nabla^c r(-\nabla_c F_{ab} + \nabla_a F_{cb} + \nabla_b F_{ca}) + \\
&+R^c_a F_{cb} + R^c_b F_{ca} - 2R_{acbd}F^{cd} + \Big(\frac{k^2}{r^2} - R\Big)F_{ab} - \\
&-\nabla_a\nabla_b F^c_c - 2n\Big(\nabla_a\nabla_b F + \frac{2}{r}\nabla_{(a}r\nabla_{b)}F\Big) - \Big[\nabla_c\nabla_d F^{cd} + \frac{2n}{r}\nabla^c r\nabla^d F_{cd} + \\
&+\Big(-R^{cd} + \frac{2n}{r}\nabla^c\nabla^d r + \frac{n(n-1)}{r^2}\nabla^c r\nabla^d r\Big)F_{cd} - \\
&-2n\Box F - \frac{2n(n+1)}{r}\nabla^c r\nabla_c F + 2(n-1)\frac{k^2 - nK}{r^2}F - \\
&-\Box F^c_c - \frac{n}{r}\nabla^d r\nabla_d F^c_c + \frac{k^2}{r^2}F^c_c\Big]g_{ab} = 16\pi\Sigma_{ab}
\end{aligned} \tag{3.35}$$

$$\frac{k}{r}\Big[-\frac{1}{r^{n-2}}\nabla_b(r^{n-2}F^b_a) + r\nabla_a\frac{F^b_b}{r} + 2(n-1)\nabla_a F\Big] = 16\pi\Sigma_a \quad if \quad k^2 \neq 0 \tag{3.36}$$

$$-\frac{1}{2}\nabla_a\nabla_b F^{ab} - \frac{n-1}{r}\nabla^a r\nabla^b F_{ab} + \frac{1}{2}\Box F^a_a + \frac{n-1}{2r}\nabla^a r\nabla_a F^b_b - \frac{n-1}{2n}\frac{k^2}{r^2}F^a_a +$$
$$+\Big[\frac{1}{2}R^{ab} - \frac{(n-1)(n-2)}{2r^r}\nabla^a r\nabla^b r - \frac{n-1}{r}\nabla^a\nabla^b r\Big]F_{ab} + (n-1)\Box F +$$
$$+\frac{n(n-1)}{r}\nabla^a r\nabla_a F - \frac{(n-1)(n-2)}{n}\frac{k^2-nK}{r^2}F = 8\pi\Sigma \tag{3.37}$$
$$-\frac{k^2}{2r^2}[2(n-2)F + F^a_a] = 8\pi\tau_T \quad if \quad k^2(k^2-nK)\neq 0 \tag{3.38}$$

3.2.3 Master variables and master equations

A truly impressive achievement in the study of quasinormal modes for static asymptotically flat black holes is the construction of a master equation that characterises them.[22, 23] A master equation is a rather simple differential operation that acts on a concrete variable, the *master* variable, which has been constructed wisely so that a mathematically complex problem simplifies into a single equation or a reduced set of equations. This is notoriously done in the study of Schwarzschild-Tangherlini quasinormal modes. Since all perturbations still occur in vacuum, the r.h.s. of all the perturbation equations of all three sectors derived in the previous section will vanish. From now on, implementing the large D limit into the previous perturbation equations will always mean making $n \to \infty$, i.e. the large D limit applies on the Einstein submanifold.

Working with Schwarzschild-Tangherlini as the background spacetime, with metric 2.4 (hence $\Theta_{\mu\nu} = 0$) and $f(r) = 1-\left(\frac{r_0}{r}\right)^{D-3}$, the master equation for Schwarzschild-Tangherlini QNM in the large D limit takes the rather simple expression

$$\Big(\Box - \frac{V_A}{1-\left(\frac{r_0}{r}\right)^{D-3}}\Big)\Phi_A = 0 \tag{3.39}$$

where Φ_A is the master variable and V_A is a potential like function; both take different expressions for the scalar, vector and tensor sectors. The master equation 3.39 is, in essence, a wave equation modelled by an external potential V_A. Our job now is to determine the expressions of V_A and Φ_A for each sector. The split of Schwarzschild-Tangherlini spacetime is done by identifying its $D-2$ sphere as the Einstein manifold. As consequence, in this particular case we'll have $K = 1$, $n = D-2$, and $(a, b, c...) = t, r$ in the usual Schwarzschild coordinates.

Tensor sector

In this case the master equation is straightforward, since by just defining $\Phi_T = r^{n/2} H_T$, then equation 3.14 takes the shape of a master equation 3.39, with potential[22]

$$V_T = \frac{f}{r}\Big[k^2 + 2 + \frac{n(n-2)}{4} + \frac{n^2}{4}\Big(\frac{r_0}{r}\Big)^{n-1}\Big] \tag{3.40}$$

where, recall, n is the dimension of the horizon submanifold, so $n = D - 2$.

Vector sector

Here, the master variable is also fast to reach. By defining $\Phi_V = r^{-n/2}\Omega$, with Ω satisfying $\epsilon^{ab}\nabla_b\Omega = r^{n-1}F_a$ in terms of the Levi-Civita tensor on the radial 2-submanifold, then equation 3.21 takes the shape of a master equation 3.39, with potential[22]

$$V_V = \frac{f}{r^2}\Big[k^2 + 1 + \frac{n(n-2)}{4} + \frac{3n^2}{4}\Big(\frac{r_0}{r}\Big)^{n-1}\Big] \tag{3.41}$$

where again $n = D - 2$ and as usual $f = 1 - (\frac{r_0}{r})^{D-3}$.

Scalar sector

For the scalar sector, as expected, the master equation is quite longer to derive. Define first a set of three variables[22] $X(t,r) = r^{n-2}(F^t_t - 2F)$, $Y(t,r) = r^{n-2}(F^r_r - 2F)$, $Z(t,r) = r^{n-2}F^r_t$. Let $X(\omega,r)$, $Y(\omega,r)$, $i\omega Z(\omega,r)$ be their respective Fourier transforms with respect to t. Define, then,

$$\Phi_S(\omega,r) = \frac{nZ(\omega,r) - r(X(\omega,r) + Y(\omega,r)}{r^{n/2-1}\big[k^2 - n + \frac{1}{2}n(n+1)\big(\frac{r_0}{r}\big)^{n+1}\big]}$$

Scalar perturbation equations take, then, the shape of

$$-f\frac{d}{dr}\Big(f\frac{d\Phi_S}{dr}\Big) + V_S\Phi_S = \omega^2\Phi_S$$

which, after a Fourier transformation back to the (t,r) space, takes the shape of a master equation 3.39. Hence, $\Phi_S(t,r) = \Phi_S(\omega,r)|_{\omega=i\partial_t}$, with a scalar potential of expression:

$$V_S = \frac{f}{16r^2H^2}\Big\{n^4(n+1)^2x^3 + n(n+1)[4(2n^2-3n+4)m + n(n-2)(n-4)(n+1)]x^2 -$$

$$- 12n[(n-4)m + n(n+1)(n-2)K]mx + 16m^3 + 4n(n+2)m^2\Big\} \tag{3.42}$$

being $m = k^2 - n$, $x = (r_0/r)^{n-1}$ and $H = m + 1/2n(n+1)x$.

3.2.4 QNM of static black holes

With as little as possible but as much as necessary detail on the mathematical resolution of the master equations, we aim now to determine the spectrum of QNM frequencies for Schwarzschild-Tangherlini in the large D limit, and hence show that they classify into two classes depending on their leading order dependence on D. Since we are interested in the frequency spectrum, we'll work with the master equation on the Fourier space for time. Then, in the large D limit, 3.39 is rewritten as[24]

$$\Big(\frac{d^2}{dr_*^2} + \omega^2 - V_A\Big)\Phi_A = 0 \tag{3.43}$$

being $dr_* = dr/f$.

Potential analysis

We begin by doing a quick qualitative analysis on the potentials V_A in 3.42, 3.41 and 3.40. In the large D limit, when $r \to r_0^+$, all three potentials tend to small finite values which are irrelevant since the potentials massively grow in other zones.

Written as a function of r_*, all potentials show a barrier that grows with the mode number ℓ, peaks and asymptotically decays when approaching infinity (see figure 3.1). Furthermore, the vector and scalar potentials have an additional minor but relevant minimum for r_* slightly smaller than the peak position[20]. The tensor potential, meanwhile, is monotonically increasing before the peak. The peaks are located at $r_* \sim 1$, so they correspond to the near zone or r, by definition of r_*. Further away the behaviour is simply asymptotically flat as expected. Evaluating for a finite mode number ℓ while applying the large D limit $n \to \infty$, the position of the peak coincides for all three positions and tends to a finite value of r_*, hence

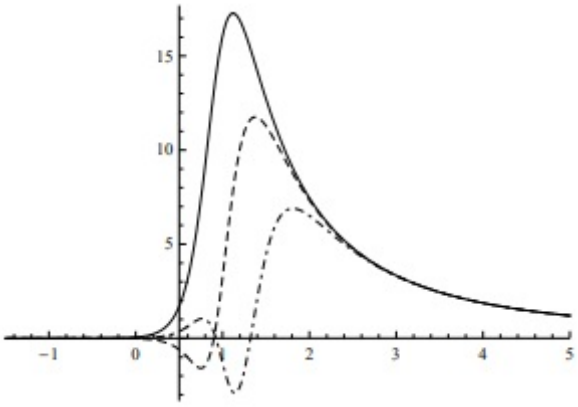

Figure 3.1: This figure is taken from [20]. It illustrates the shape of $V(r_*)$ for finite $n = 7$ and ℓ_2. Solid, dashed and dot-dashed plots correspond to tensor, vector and scalar potentials respectively. Note how the tensor potential has no minimum while the others do. Decoupled modes will be localised left from the peak (the horizon is at $r_* = -\infty$); non decoupled modes to the right of the peak.

in the near region, and the value of the maximum diverges at $D \to \infty$, growing as $V = n^2\omega_c$, being $\omega_c = \frac{1}{2r_0}\left(1 + \frac{2\ell}{n}\right)$[20].

Furthermore, the position of the minimum of the scalar and vector potentials also shrinks onto the peak position. The direct consequence of this behaviour is that, in the large D limit, an infinite barrier appears between the near and far regions, so modes with finite ω will be confined in a narrow interval in the near zone (since we assume no modes come from asymptotically flat infinity). That's the qualitative justification behind decoupled $\omega \sim 1/r_0$ QNM being strongly localised in the near zone and vanishing further away, with non decoupled modes behaving oppositely. Both families are fully separated at large D precisely after this infinite barrier in the potential.

Near and far zone solutions

We will, without great detail, summarize the discussion that leads to the frequency spectrum of Schwarzschild-Tangherlini QNM, based on the development in [20]. The master equation, despite being a huge simplification of the problem, is not fully ana-

lytically solvable yet due to the V_A term. Approximate expressions arise from solving Φ_A separately in the near and far zones with their respective boundary conditions; we may then choose solutions from each region that can match in the overlapping region. Explicit expressions of the approximate solutions are long and beyond our interest, so we'll skip them. Being 3.43 a second order ordinary homogeneous equation in r (or r_*), the general solution is always a linear combination of two independent solutions, $\Phi = A_+\Phi^+ + A_-\Phi^-$. It can be proved[20] that normalizable solutions in both regions cannot match for frequencies higher than ω_c.

In the far zone, the master equation can be solved over flat space. Regularity implies, if $|\omega| < n\omega_c$, that the coefficients are related by

$$\left|\frac{A_+}{A_-}\right| = e^{2nr_0 Ref(\omega/\omega_c)}$$

being $f(z) = log\frac{1+\sqrt{1-z^2}}{z} - \sqrt{1-z^2}$ a complex function. In particular, for $\omega \to n\omega_c^-$ so that $\omega_c - \omega/n \sim 1/n^{2/3}$, then solutions of take a simpler form $\Phi = A + B\log\frac{r}{r_0}$ at leading order. The solution is only valid is the coefficients satisfy

$$\left|\frac{A}{B}\right| \sim \frac{1}{n}$$

at leading order.

Meanwhile, in the near, zone, solutions for all the sectors are related to hypergeometric functions (directly in the tensor and vector case, under an operator in the scalar case). Checking their assymptotic behaviour for large r, i.e. in the overlapping zone, we get relations for the coefficients in all the regimes of $\omega < n\omega_c$:

$$\left|\frac{A_+}{A_-}\right| \sim \left|\frac{A}{B}\right| \sim O(1)$$

with different dependence on D than the expressions for the far zone.

This radically different behaviour is what constrains and quantises the values of ω.

Non decoupled spectrum

We try to match the solutions for $\omega_c - \omega/n \sim n^{-2/3}$. The different dependence of A/B in each zone quantises the spectrum, since the only acceptable values of ω will be those for which $A = A(\omega) = 0$ in the far zone. Since it can be proved that, there, $A(\omega)$ is of the type of an Airy function of the difference $\omega_c - \omega/n$, the multiplicity of its zeros and the expression B can be proved to be the appropriate so that $\left|\frac{A_+}{A_-}\right| \sim \left|\frac{A}{B}\right| \sim O(1)$ in the far zone too. Hence, the spectrum of $\omega_c - \omega/n$ will be the known zeros, $-a_k$, of the Airy function. Taking in mind all the factors, we have:

$$\left(\frac{2n^2 r_0^2}{e^{i\pi}\omega_c}\right)^{1/3)}\left(\omega_c - \frac{\omega_k}{n}\right) = a_k \approx \left[\frac{3\pi}{8}(4k-1)\right]^{2/3} \tag{3.44}$$

being k natural. Simplifying and isolating *omega*, we finally get the non decoupled spectrum:

$$\omega_{\ell,k} r_0 = \frac{n}{2} + \ell - a_k\left(\frac{e^{i\pi}}{2}\left(\frac{n}{2}+\ell\right)\right)^{1/3} \sim O(n) \tag{3.45}$$

Lastly, we get information about how quickly these modes vanish (or grow) with time by examining the imaginary part of the frequencies. In this case, the ratio between imaginary and real part of 3.45 is

$$\frac{Im\omega}{Re\omega} \sim n^{-2/3} \tag{3.46}$$

which means that, in the large D limit, the dissipative term due to $Im\omega$ is much smaller in comparison, so non decoupled QNM will be long lived. The modes are universal for many different black hole configurations, including all asymptotically flat, static and spherically symmetric black holes[25].

Decoupled spectrum

The decoupled spectrum development diverges from the previous non decoupled spectrum from the beginning. Now, we match the behaviours in near and far zone in the most direct way possible: by setting $A_+ = 0$, so that $\Phi \propto \Phi^-$, which is normalizable. Since these solutions are then localised only into the near region, a standard perturbative expansion will be enough to solve the equation by variation of the constants. There will be no need to solve the far zone anymore. Decoupled

QNM are static at leading order, so we need to specify one higher order in $1/n$ to find the frequency spectrum.

According to our boundary conditions, $\Phi \propto r^{-1/2}$ at $r \to \infty$ and regularity at the horizon, no solution emerges from the tensor sector. Contrary, a solution exists from the vector sector, and by comparing the higher order terms, we get its frequency, $\omega r_0 = -i(\ell - 1)$ purely imaginary at higher order, and expansion into even higher orders will raise more corrections:

$$\omega r_0 = -i(\ell-1)\Big(1 + \frac{1}{n}(\ell-1) + \frac{2}{n^2}(\ell-1)\big(\frac{\pi^2}{6} - 1\big)\Big) + O(1/n^3) \tag{3.47}$$

where, as expected, ω is independent of n at leading order.

Repeating essentially the same steps for the scalar sector, we achieve frequencies with expression

$$\omega r_0 = \pm\sqrt{\ell-1}\Big(1 + \frac{1}{n}\big(\frac{3\ell}{2} - 2\big)\Big) - i(\ell-1)\Big(1 + \frac{1}{n}(\ell-2)\Big) + O(1/n^2) \tag{3.48}$$

again independent on the dimensionality at leading order and no longer purely imaginary. This completes the spectrum of QNM in the large D limit of Schwarzschild-Tangherlini black holes.

3.3 The Gregory-Laflamme instability

The second half of this chapter will be dedicated to the Gregory-Laflamme instability, a major result regarding stability of black branes and black strings that we will recover again afterwards with the use of effective theories.

3.3.1 Mechanical justification

According to black hole mechanics, the stability of a state against a possible evolution into a different state will depend on the sign of the area difference between them, given the second law:

$$dA > 0 \tag{3.49}$$

The area of a Schwarzschild-Tangherlini black hole is $A_{BH} = r_0^{D-2}\Omega_{D-2}$, and its mass $M_{BH} = \frac{(D-2)r_0^{D-3}\Omega_{D-2}}{16\pi G}$. For a black string, its area per unit length (along the free direction) is[5] $A_{BS} = r_0^{D-3}\Omega_{D-3}$ and its mass per unit length, $M_{BS} = \frac{(D-3)r_0^{D-4}\Omega_{D-3}}{16\pi G}$. We can compare then the rate of grow $\frac{d\log A}{d\log M}$ for each case, easily finding

$$\log A \sim \frac{D-2}{D-3}\log M \quad Hole \tag{3.50}$$

$$\log A \sim \frac{D-3}{D-4}\log M \quad String \tag{3.51}$$

Since the growing rate is always larger for the black hole for finite $D > 4$, we may then expect $A_{BH} > A_{BS}$, i.e. a stable black hole, at low energies, which is essentially the Gregory-Laflamme instability, while $A_{BH} < A_{BS}$, i.e. a stable black string, at high energies. The equilibrium point will lie, by explicit calculation, at

$$r_0^{BS} = \frac{D-2}{D-3}r_0^{BH} = L\Big(\frac{D-2}{D-3}\Big)^{D-2}\frac{\Gamma\big(\frac{D-1}{2}\big)}{\sqrt{\pi}\Gamma\big(\frac{D}{2}-1\big)} \tag{3.52}$$

where L is the length of the string. Hence, the radius of the black hole must be lower or equal than L for all finite $D > 4$, and this constrains the values of D for which the phase transition might happen to $D \leq 13$. Otherwise, no stable black holes are expected to be found near the transition point of the hole-string phase diagram[5].

3.3.2 Derivation

Consider the usual metric of a black p-brane

$$ds^2 = -f(r)dt^2 + \frac{dr^2}{f(r)} + r^2 d\Omega_{D-p-2} + dx_i dx^i, \tag{3.53}$$

where i runs over $1, ..., p$, and $f(r) = 1 - \left(\frac{r_0}{r}\right)^{D-p-3}$. We want to study its stability against metric perturbations. To this purpose, we will apply the gauge invariant perturbation formalism developed in the previous section, by identifying the p flat worldvolume directions as the Einstein manifold with respect to which we develop the scalar, vector and tensor sectors. Hence, we'll have a particular case of the perturbation formalism where $n = p$, $K = 0$ and $r(y^a) = 1$, since the unperturbed metric over the worldvolume of the brane is flat; $r(y^a)$ follows the general notation in 3.1. In order to preserve the notation, we've already used the Latin indices accordingly in 3.53: $(i, j, k...) = 1, ..., p$.

We are interested in the study of possible unstable solutions. We'll assume spherical symmetry in the perturbations for further simplicity. Then, the metric fluctuation must have the following expression:

$$h_{\mu\nu} = e^{\Omega t} H_{\mu\nu}(r, x^i) \tag{3.54}$$

with real $\Omega > 0$ so that the perturbation grows with time and leads to an instability. The next step will consist in particularising tensor, vector and scalar Einstein equations for perturbations to the $D-p$ dimension Schwarzschild-Tangherlini black hole background metric with the mentioned ansatz for $h_{\mu\nu}$.

Imposing continuity on r and regularity at both the horizon and infinity, we realise that both tensor and vector components of $h_{\mu\nu}$ must vanish if the mentioned ansatz is assumed, i.e. $H_{ij} = H_{ia} = 0$[26]. Hence, only the scalar sector is not trivial. The general formalism is greatly reduced due to the mentioned simplifications: from 3.28, we see that $H_{ij} = 0 \Rightarrow H_T = H_L = 0$, $H_{ai} = 0 \Rightarrow f_a = X_a = F = 0$, so the only non vanishing gauge invariant quantity is $F_{ab} = f_{ab}$, where $h_{ab} = f_{ab} S(x^i)$ and $S(x^i)$ is a scalar harmonic eigenfunction, only dependent on the worldvolume coordinates. Hence, comparing notations, we see that $f_{ab} \propto H_{ab}$. We further assume the perturbation is transverse and traceless in the S-T space, i.e. $\nabla_c f^c_a = f^c_c = 0$. Then, the vast Einstein scalar equation 3.35 in the S-T background dramatically reduces to

$$\Box f_{ab} + 2R_{acbd} f^{cd} - k^2 f_{ab} = 0 \tag{3.55}$$

which can also be written covariantly in the whole D-spacetime as

$$\nabla_\alpha \nabla^\alpha h_{\mu\nu} + 2R_{\mu\nu\alpha\beta}h^{\alpha\beta} = \Delta_L h_{\mu\nu} = 0 \tag{3.56}$$

which is a particular case of the more general Lichnerowicz equation[27] that governs the fluctuation of the Ricci tensor in terms of the metric fluctuation.

In this pàrticular case where $K = 0$, the scalar harmonic eigenfunctions obey 3.24 with $\Delta = \partial^i \partial_i$ since $g_{ij} = \delta_{ij}$. Hence, the eigenfunctions are the trivial $S(x^i) = e^{ik_j x^j}$. Relabelling that $h_{ab} = f_{ab}S(x^i) = e^{\Omega t}F_{ab}(r)S(x^i)$, Einstein equations are decoupled with respect to F_{tr}[26]. Naming $n = D - p - 3$:

$$\begin{aligned}
&\Big\{ -\Omega^2 - \mu^2 f + \frac{n^2(1-f)^2}{4r^2} \Big\} F^{tr\prime\prime} + \Big\{ \mu^2[(n+1) - 2(1-f) - (n-1)(1-f)^2] + \\
&+ \frac{\Omega^2[(n+1) + (2n-1)(1-f)]}{rf} + \frac{3n^2(1-f)^2[(n+1) - (1-f)]}{4r^3 f} \Big\} F^{tr\prime} + \\
&+ \Big\{ (\mu^2 + \Omega^2/f)^2 + \frac{\Omega^2 4(n+1) - 8(n+1)(1-f) - (5n^2 - 4n - 4)(1-f)^2}{4r^2 f^2} + \\
&+ \frac{\mu^2[4(n+1) - 4(3n+2)(1-f) + (n^2 + 8n + 4)(1-f)^2]}{4r^2 f} + \\
&+ \frac{n^2(1-f)^2[(n+1)(2n+1) - (n+2)(n+1)(1-f) + (1-f)^2}{4r^4 f^2} \Big\} F^{tr} = 0
\end{aligned} \tag{3.57}$$

which, although long, is only a decoupled ODE for $F_{tr}(r)$. As usual, $f(r) = 1 - (\frac{r_0}{r})^n$. Notoriously, ther is a regular asymptotic solution at infinity of the form $e^{-\sqrt{\Omega^2 + k^2}r}$ and also on the horizon, of the form $(r - r_0)^{-1 \pm r_0 \Omega/n}$. Apparently there's a divergence on the horizon, but that's entirely a consequence of the limitations of Schwarzschild coordinates. We will first need to transform the solution into Kruskal coordinates (T, R)[26]. Then, the transformed components TT and RR tend to $h_{TT} \approx h_{RR} \propto \pm(R \pm T)^{\Omega r_0/n - 2}$, and $h_{TR} \propto (R \pm T)^{\Omega r_0/n - 2}$. Now it is immediate that regularity on the future event horizon, at $R = T$, requires both the $+$ sign and $\Omega > 0$ so that the exponent stays positive. We are done: recalling 3.54, a positive real frequency $\Omega > 0$ will make the perturbation to grow with time and, so, spacetime will be unstable. The Gregory-Laflamme instability emerges as a particular unstable solution to Einstein perturbation equations with a Schwarzschild-Tangherlini brane background geometry.

Chapter 4

Effective theories of large D black holes

4.1 Motivation and generalities

As seen in the previous chapter, black hole metric perturbations in the form of quasinormal modes can be split and classified into two groups: decoupled modes, for which $\omega \sim 1/r_0$, and non decoupled much faster modes, for which $\omega \sim D/r_0$. In particular, the $\sim 1/r_0$ slow modes are fully localized near the horizon, i.e. $r - r_0 << r_0$, being decoupled in the far zone at all orders in D[28]. The usefulness of an effective theory arises then from the possibility of evaluating the dynamics of black holes at long distances by integrating into some effective functions all the near zone effects[5][28], achieving a theory which is now able to carry on a non linear study of the decoupled dynamics in the far zone, deeper than the always linear previous study of quasinormal modes.

Again, the large D limit plays a key role in the development of an effective theory. As mentioned in previous chapters, black hole dynamics at finite D are impossible to solve analytically due to the absence of characteristic length scales besides the Schwarzschild radius r_0, and the construction of an effective theory requires a separate treatment of a near zone, whose dynamics are integrated and hidden in the

parameters of the theory, and a far zone where the theory applies. A possibility would be to study the dynamics directly far from the black hole considering it, effectively, as a point particle, as the background curvature curvature radius is much larger than the black hole size $\sim r_0$.[5] Nevertheless, this approach will omit all the dynamics regarding the black hole horizon and its fluctuations, so it's not useful in order to study metric perturbations from a black hole spacetime. Fortunately, the large D limit directly provides us with a second length scale r_0/D that enables to treat separately the near and far zone with respect to the horizon, giving rise to the effective theory.

Mainly, two different effective theories have been developed in parallel being based on the large D limit.[5] Below, we will discuss each of them in sections 4.2 and 4.3 respectively and we'll follow their path to their final effective equations; despite apparently very different, both theories remarkably coincide on, most importantly, the values of quasinormal frequencies. The fact that two different effective theories can emerge to describe the same phenomena is due to deeply different initial assumptions on the metric ansatz that is used as the starting point for the derivation of the equations. In concrete, both theories split spacetime in two submanifolds and calculations are done with tensors in one of the those submanifolds. However, the split is radically different between the theories, breaking direct parallelisms and leading to different effective equations.

4.2 Membrane effective theory

4.2.1 Ansatz and motion equations

The first of the two effective theories that parallelly arise thanks to the large D limit is the membrane theory. Consider a spacetime with $D = p + n + 3$ dimensions with $SO(n+1)$ symmetry. [29] Then the metric takes the form

$$ds^2 = g_{\mu\nu}dx^\mu dx^\nu + e^\phi d\Omega_n = g_{\mu\nu}(x^\mu)dx^\mu dx^\nu + e^{\phi(x^\mu)}\gamma_{ij}(x^i)dx^i dx^j \qquad (4.1)$$

where Greek indices run over $1, ..., p+3$, Latin indices over $1, ..., n$, and $d\Omega_n = \gamma_{ij}(x^i)dx^i dx^j$ is the metric of a unit radius n-sphere. Due to this splitting timelike, radial and worldvolume dimensions will be treated separately from the n spherically symmetric directions.

From now on, ∇_μ will denote covariant derivatives on the $p+3$ submanifold, and Greek indices will be raised and lowered with $g_{\mu\nu}$. Einstein equations give rise to motion equations for both the unknown metric $g_{\mu\nu}$ and the scalar field ϕ; it can be easily proved that they are the following:

$$R_{\mu\nu} = \frac{n}{2}\nabla_\mu\nabla_\nu\phi + \frac{n}{4}\nabla_\mu\phi\nabla_\nu\phi \tag{4.2}$$

$$(n-1)e^{-\phi} = \frac{1}{2}\nabla^2\phi + \frac{n}{4}(\nabla\phi)^2$$

Here, $R_{\mu\nu}$ is the Ricci tensor on the $p+3$ submanifold, hence not necessarily zero by Einstein equations.

We'll look for solutions of 4.2 in the large D limit for fixed p, hence $n \to \infty$ throughout the whole derivation[29]. The first equation in 4.2 relates the length scale of metric variations and that of the scalar field. On the left hand side we have only metric derivatives, each of them inversely proportional to the metric characteristic length ℓ_g. The curvature tensor terms have the form of either $\partial^2 g$ or $(\partial g)^2$. Hence, $R_{\mu\nu} \sim \ell_g^{-2}$. For the right hand side, assume each field derivative is inversely proportional to a field characteristic length ℓ_ϕ. Given that $\nabla_\mu\nabla_\nu\phi = \partial_\mu\partial_\nu\phi - \Gamma^\rho_{\mu\nu}\partial_\rho\phi$, we'll have terms escalating as $\sim n\ell_\phi^{-2}$ and terms as $\sim n\ell_\phi^{-1}\ell_g^{-1}$.

For equality to hold in 4.2, then, metric and field derivatives must escalate differently: we need $\ell_g << \ell_\phi$ in the large D limit, so spacetime will be governed by two different length scales, heuristically originated on the fact that ϕ encodes the size of a $n \to \infty$ sphere, so its derivatives are more "expensive"[29] that the metric ones. Reached that conclusion, it is evident that dominant terms in the right hand side must be those that escalate as $\sim n\ell_\phi^{-1}\ell_g^{-1}$, i.e. only the Christoffel term. Consequently, the large D limit reduces 4.2 to $R_{\mu\nu} \approx -\frac{n}{2}\Gamma^\rho_{\mu\nu}\partial_\rho\phi$ and we may now infer

that, for equality to still hold, the length scales must be directly related;

$$R_{\mu\nu} \approx -\frac{n}{2}\Gamma^{\rho}_{\mu\nu}\partial_{\rho}\phi \Rightarrow \ell_g \sim \frac{1}{n}\ell_\phi << \ell_\phi \tag{4.3}$$

We still have the freedom of choosing a coordinate chart. We require a chart $\{x^\mu\}$ for which both the metric and the field are order unit, and $\partial g \sim n$, $\partial\phi \sim 1$. A problem then arises from the fact that a metric with $O(1)$ values and length scale $1/n$ would become trivial, since this is a point particle limit and no interesting physical results would emerge. We avoid the issue by applying a coordinate transformation and working, afterwards, with a conformal metric[29]. Each chart will only have a domain of order $1/n$ around a point, so we should repeat the process until the overlaps cover the whole $p+3$ submanifold:

$$x^\mu = x_0 + \frac{1}{n}\alpha^\mu_a y^a; \alpha \sim O(1) \tag{4.4}$$

$$g_{\mu\nu} = n^2\alpha^a_\mu\alpha^b_\nu g_{ab} \equiv \alpha^a_\mu\alpha^b_\nu G_{ab} \sim O(1)$$

$$\chi_a \equiv n\nabla_a\phi = \alpha^\mu_a\nabla_\mu\phi \sim O(1)$$

Our next step is to apply these transformations to the equations of motion 4.2 so that all the dependence on n is isolated into explicit n factors and Christoffel symbols. We achieve it by expressing everything in terms of the conformal metric G_{ab} for contractions and raising indices and the dilaton χ_a, both of order unit. By applying the transformations, the equations are rewritten as:

$$R_{ab} = \frac{1}{2}\nabla_a\chi_b + \frac{1}{4n}\chi_a\chi_b \tag{4.5}$$

$$\frac{1}{2}\nabla^a\chi_a = \frac{n-1}{n}e^{-\phi} - \frac{1}{4}\chi^2$$

In the first equation and after applying the conformal change in both sides, the second term on the r.h.s. and the dilaton derivative are order $1/n$ and hence vanish. The same applies to the l.h.s. on the second equation. Thus, in the large D limit, the previous equations 4.5 simplify to

$$R_{ab} = -\frac{1}{2}\Gamma^c_{ab}\chi_c \tag{4.6}$$

$$-G^{ab}\Gamma^c_{ab}\chi^c = 4e^{-\phi} - \chi^2$$

at leading order. Thanks to this basis change, the coordinates are now suitable to describe the worldvolume dynamics.

4.2.2 Black brane and membrane solutions

A part from a trivial flat solution which only requires $e^{\phi}\chi^2 = 4$, a black brane like solution to 4.6 arises with the expression[29]

$$G_{ab} = \Big(\eta_{ab} + e^{-R}O_a O_b\Big)dx^a dx^b \tag{4.7}$$

where R is one spacelike coordinate and O is a null one-form with respect to flat space. 4.7 metric, characterising only the non spherical submanifold (indices run to $1, ..., p+2$), solves Einstein equations 4.6 at leading order provided that $e^{\phi}\chi^2 = 4$, $(2dR - d\chi)dR = (2dR - d\chi)O = 0$. We'll use this result later.

Now we define a scalar $SO(n+1)$ invariant field $B(x^\mu)$ with respect to a flat metric whose zeros have topology of sphere times time[29], and whose positive region includes infinity. We'll then name as *membrane* the submanifold where $B = 0$. We also require $\partial_\mu B \partial^\mu \phi > 0$. Consider also a null $SO(n+1)$ invariant one-form O_μ which satisfies $\eta^{\mu\nu}O_\mu O_\nu = 0$, where $\eta_{\mu\nu}dx^\mu dx^\nu$ is the metric of $p+3$ dimensional flat space. We also define a second scalar

$$\psi = 1 + B\frac{\partial_\mu B \partial^\mu \phi}{2\partial_\mu B \partial^\mu B} \tag{4.8}$$

whose definition is motivated by a simplification of the metric once we express it in terms of ψ rather than B: as long as the mentioned properties and $O^\mu\Big(\frac{1}{2}\partial_\mu\phi - \partial_\mu\psi\Big) = 0$ are satisfied, the black brane metric[29]

$$g_{\mu\nu} = \eta_{\mu\nu} + \frac{O_\mu O_\nu}{\psi^{D-3}} \tag{4.9}$$

will be a solution of 4.6 because, as we'll shortly see, the expression and the required properties mirror those of the known solution in 4.7. By inspection we see that the membrane $B = 0$ corresponds to $\psi = 1$, and the outside (region including ∞) and inside, to $\psi > 1$ and $\psi < 1$ respectively.

At leading order in the large D limit, Einstein equations are solved trivially everywhere on the outside except the *membrane region*, described by

$$\psi - 1 \sim 1/D \Leftrightarrow \log\psi \sim \psi - 1 \Leftrightarrow \psi^{D-3} \sim e^{(D-3)(\psi-1)} \tag{4.10}$$

However, after a new coordinate chart that includes $R = n(\psi - 1)$ as directly one of the new coordinates and conveniently rescaled as in 4.4, in the membrane region 4.10 the metric 4.9 takes the form of 4.7, which is solution of Einstein equations 4.6 at leading order in $1/D$.[29]

4.2.3 Equivalent metrics

The fact that 4.9 solves Einstein equations only at leading order indicates that we may treat as equivalent several metrics which only differ at higher orders.[29] Since, at leading order, ψ^{D-3} vanishes everywhere outside the membrane, we shall treat as equivalent the metrics with O_μ and $O_\mu + \delta O_\mu$ as long as the difference vanishes on the membrane, $\delta O_\mu|_{B=0} = 0$. Similarly, a global rescaling of the scalar B leaves invariant ψ by construction, which is the only place where B appears in the metric. Hence, we shall also treat as equivalents B and αB, for some constant α. We may, then, freely choose a representative of each equivalence class for both B and O and work always with them. It's convenient to pick them so that O is parallelly transported along a the congruence of the gradient of B field and so that these congruence are affinely parametrized geodesics:[29]

$$\nabla^\nu B \nabla_\nu \nabla_\mu B = \nabla^\nu B \nabla_\nu O_\mu = 0 \tag{4.11}$$

which easily implies dB to be constant in modulus, which we fix to unit after rescaling.

As a last consideration before the correction, rewrite the metric 4.9 as

$$ds^2 = \left(\eta_{ab} + \frac{O_a O_b}{\psi^{D-3}}\right) dx^a dx^b + \left(1 + \frac{O_S O_S}{\psi^{D-3}}\right) dS^2 \tag{4.12}$$

specifying as a coordinate the radial direction of the $SO(n+1)$ symmetry, i.e. $S^2 = e^\phi$. Here, then, Latin indices run over $1, ..., p+2$, including the timelike

coordinate. In order to emphasize the special role of coordinate S, we'll express $O = O_\mu dx^\mu = e^{-h}(dS - u_a dx^a)$, so that the metric depends, at the moment, on $\{B, h, u_a\}$, two scalars and one one-form in the $p+2$ (recall, not $p+3$) submanifold. Moreover, $O^2 = 0$ in $p+3$ flat space implies $u^2 = -1$, constant, in $p+2$ flat space.

4.2.4 First order correction

Our objects, whose relations we aim to determine, are $n_\mu = \partial_\mu B$, u_μ and h. Define $K_{\mu\nu} = \nabla_\mu n_\nu$. In addition, one-forms $\{u, n, dS\}$ define a 3-dimensional subspace on the $p+3$ tangent space consisting in the radial direction dS, the normal direction to the membrane $dB = n$ and the direction tangential to the worldvolume velocity u. We may, then, classify all possible contractions between our objects depending on their tensor class in the remaining p dimensional subspace, orthogonal to $\{u, n, dS\}$[29]:

- Scalars S_A: K_{ss}, $u^\mu K_{s\mu}$, $u^\mu u^\nu K_{\mu\nu}$, $P^{\mu\nu}K_{\mu\nu}$, $\partial_s h$, $u^\mu \partial_\mu h$, $P^{\mu\nu}\nabla_\mu u_\nu$.
- Vectors V_A^μ: $P^{\mu\alpha}\nabla_s u_\alpha$, $P^{\mu\alpha}u^\nu \nabla_\nu u_\alpha$, $P^{\mu\alpha}K_{s\alpha}$, $P^{\mu\alpha}u^\nu K_{\nu\alpha}$, $P^{\mu\alpha}\partial_\alpha h$.
- Symmetric tensors $T_A^{\mu\nu}$: $P^{\mu\alpha}P^{\nu\beta}\Big(K_{\alpha\beta} - \frac{\eta_{\alpha\beta}}{p}P^{\rho\sigma}K_{\rho\sigma}\Big)$ and $P^{\mu\alpha}P^{\nu\beta}\Big(u_{(\alpha\beta)} - \frac{\eta_{\alpha\beta}}{p}P^{\rho\sigma}K_{\rho\sigma}\Big)$.
- Antisymmetric tensor $A^{\mu\nu} = P^{\mu\alpha}P^{\nu\beta}u_{[\alpha\beta]}$.

We'll use a convenient basis that directly separates the already mentioned 3 dimensional subspace, by using $d\psi$, $dS - Sd\psi$ and O as elements of the dual basis. The remaining p basis elements will be given by $P^\mu_\nu dx^\nu$, being $P^{\mu\nu}$ a projector orthogonal to dS, $d\psi$ and O. The metric will then be a linear combination of symmetrized tensor products (expressed with $\times$) of those forms. In this basis, though, some elements may immediately vanish after a gauge choice[29], so that $d\psi \times (dS - Sd\psi)$ is the only non vanishing element containing $d\psi$. The most general form the metric may have up to first order will then be

$$ds^2 = \eta_{\mu\nu}dx^\mu dx^\nu + \frac{O\times O}{\psi^{D-3}} + \frac{1}{n\psi^n}\Big(K_1(x)O^2 + 2K_2(x)O\times(dS - Sd\psi) + K_3(x)(dS - Sd\psi)^2 + \tag{4.13}$$

$$+2K_4(x)d\psi \times (dS - Sd\psi) + 2Q_1^\beta(x)O \times P_{\beta\mu}dx^\mu + 2Q_2^\beta(x)(dS - Sd\psi) \times P_{\beta\mu}dx^\mu +$$
$$+T^{\alpha\beta}(x)P_{\alpha\mu}P_{\beta\nu}dx^\mu dx^\nu\Big) + O\Big(\frac{1}{n^2}\Big)$$

in terms of four scalar functions K_a, two vectors Q_a and one symmetric tensor T whose expressions will be determined by solving Einstein equations at first order in $1/n$. Each of these functions can be expressed as linear combinations of the previously mentioned tensors from their same class:

$$K_a = \sum_{A=1}^{7} K_a^A(\psi)S_A(x) \tag{4.14}$$

$$Q_a^\mu = \sum_{A=1}^{5} Q_a^A(\psi)V_A^\mu(x) \tag{4.15}$$

$$T_a^{\mu\nu} = \sum_{A=1}^{2} T_a^A(\psi)T_A^{\mu\nu}(x) \tag{4.16}$$

The key fact will be that the coefficient functions of these linear combinations will only be functions of ψ, i.e. functions of $R = n(\psi - 1)$ after making the 4.4 rescaling, since their derivatives with respect to the rest of the membrane coordinates will be order $1/n^2$, hence negligible.[29]

4.2.5 Effective equations

The final result of the membrane theory will be a pair of one scalar equation and one p dimensional vector equation (living in the orthogonal p subspace). We will not deeply follow every step of the solving process of Einstein equations but we'll briefly comment them. The first step is to express the metric and the Ricci tensor in terms of exclusively rescaled coordinates around an arbitrary membrane point x_0 following 4.4: $R = n(\psi - 1)$, $V = ne^{h(x_0)}O_\mu(x_0)(x^\mu - x_0^\mu)$, $Y = n(S - s_0\psi)$ and $y^i = nP_\mu^i(x_0)(x^\mu - x_0^\mu)$, where $s_0^2 = e^\phi$ on the membrane at leading order. Working the Ricci tensor in this same basis directly decouples the equations between the scalar, vector and tensor functions.

Looking at the scalar components of Einstein equations 4.2, a fortunate linear combination of their terms leads to an ordinary and solvable equation for the coefficient functions $K_2^A(R)$. Its integration constant is determined requiring regularity at large R. However, a simple pole at $R = R_0$ on the integrand of $K_2^A(R)$ raises a multivalued component proportional to $\log(R - R_0)$ which must vanish for the solution to be physical. It is this last imposition that leads to the **scalar membrane equation**:

$$K_{\mu\nu}(U^\mu - U^\rho n_\rho n^\mu)(U^\nu - U^\rho n_\rho n^\nu) + \frac{n_S}{S}(n_S^2 + 1) = 0 \tag{4.17}$$

being $U = dS + n_S^2(dS - u)$.

Looking at the vector components of Einstein equations 4.2, again a fortunate linear combination of the equations lead to an ordinary and solvable equation for the coefficient functions $Q_2^A(R)$. Its solution, after integration, shows an unavoidable logarithmic dependence in R, with no polynomial terms after developing. Hence, it is required to have $Q_2^A(R) = 0$, which after substitution, leads to the **vector membrane equation**:

$$P_a^b(U^c - U^\mu n_\mu n^c)\nabla_c u_b = 0 \tag{4.18}$$

being again $U = dS + n_S^2(dS - u)$. Latin indices run over $1, ..., p$, since non orthogonal components of 4.18 are trivial and irrelevant.

Together, the set of $p + 1$ equations from 4.17 and 4.18 are differential equations on also $p + 1$ variables: the membrane shape $B(x)$, in the equations inside $n = dB$ and $K = \nabla n$, hence up to second order, and the velocity u, first order, which has only p degrees of freedom since $u_S = 1$, $u^a u_a = -1$ and $u^\mu n_\mu = n_S - \frac{1}{n_S}$. Given an initial shape B_0, an initial change rate n_0 and an initial velocity u_0, the **effective membrane equations** solve the non linear dynamics of the decoupled quasinormal modes of a black hole in the large D limit.

4.3 Effective theory for black branes

4.3.1 Approach

The following effective theory, despite lacking from part of the elegant covariant expressions of the previously explained membrane theory, is equally efficient at describing the non linear dynamics of the slow decoupled quasinormal modes of black holes and its effective equations are far more intuitive and easier to solve both analytically and numerically. It deeply relies on a fluid-like description of the black hole horizon, again embedded on a black brane, so we will intercalate its development with bits and details of relativistic hydrodynamics. Afterwards, in this Dissertation we will focus on the applications of this effective theory. That is why the following section will be detailed in its development, given the relevance of their results for the following chapter.

This discussion will only contemplate asymptotically flat geometries, though a parallel development can also be built in Anti-de Sitter spacetime.

4.3.2 (D-1)+1 decomposition

This introductory section briefly describes the formalism we will use to derive the effective equations, the $(D-1)+1$ decomposition; it is constantly used in Hamiltonian formulation or Arnowitt-Deser-Misner (ADM) approach of General Relativity[30], which is a parallel and analogous development of General Relativity to the Lagrangian formulation we have always been using, the latter based on minimizing a given action and treating spacetime as a field theory with the metric tensor as the dynamical object[30]. Like all Hamiltonian formulations in other areas, we require the setting of a preferred time variable, hence breaking the local $SO(D-1,1)$ symmetry, i.e. the diffeomorphism symmetry, that had been characterizing Einstein gravity up until now. Similar tools are used in Kaluza-Klein metrics[31, 32, 33], since Kaluza-Klein theory couples gravity with electromagnetism by adding a spe-

cial extra dimension related to the electromagnetic field.

Hence we assume spacetime to be foliated as a manifold with metric [34]

$$ds^2 = (-\alpha^2 + \beta^i\beta^j\gamma_{ij})dt^2 + \beta_i dt dx^i + \gamma_{ij}dx^i dx^j \tag{4.19}$$

where Latin indices run $1, ..., D-1$ and raised and lowered with γ_{ij} and its inverse γ^{ij}. This notation is, obviously, not locally $SO(D-1,1)$ covariant.

A foliation like the presented in 4.19 enables us to define a geometric extrinsic curvature tensor as[30]

$$K_{ij} = \frac{1}{\alpha}\Big(\nabla_{(i}\beta_{j)} - \frac{1}{2}\partial_t\gamma_{ij}\Big) \tag{4.20}$$

where ∇ is the covariant derivative on the $D-1$ Riemannian subspace. An intuitive explanation of this new object is neat: moving along a given submanifold of spacetime, one may feel effects of curvature even if both the spacetime and the isolated submanifold are completely flat, but just because of how the geometry of the embedding spacetime affects the geometry on the submanifold. As an example, the surface of a cylinder has zero intrinsic curvature since, naively, it can be constructed from a flat piece of paper. Nevertheless, considering the same cylinder now embedded in a 3 dimensional Euclidean space, an observer may note the effect of curvature not because of the intrinsic properties of the cylinder but because how the Euclidean geometry background affects it. Hence we would have $R_{ij} = R = 0$ but some $K_{ij} \neq 0$ and the scalar extrinsic curvature $K = \gamma^{ij}K_{ij} > 0$.

All curvature tensors may be computed from 4.19, and Einstein equations $G_{\mu\nu} = 8\pi T_{\mu\nu}$ will be given by a set of one scalar equation from component tt, $D-1$ vector equations from components ti and $(D-1)(D-2)/2$ tensor equations from components ij. Note that, even in vacuum, the curvature tensor R_{ij} in the $D-1$ subspace doesn't need to straightly vanish.

Note, finally, that despite the previous discussion has assumed a foliation in which we treated separately the timelike coordinate, a totally analogous development is

entirely possible by separating one spacelike coordinate and working in a $(D-2,1)$ Lorentzian manifold as the subspace. That is, in fact, what is going to be used in the following section.

4.3.3 Ansatz and dynamic equations

Here we start the mathematical development which will eventually lead to the effective equations. The general path to follow is very similar to that of the membrane equations deduction. We start by building an ansatz metric, we discuss the dependence on D of the coordinate chart, we solve Einstein equations at leading order of the large D limit in terms of some objects in the metric components and, finally, we let them fluctuate and we reach their dynamical equations from solving again Einstein equations, not up to a first order correction in $1/D$.

We start with an ansatz of the shape[12]

$$ds^2 = (N^2 + N^\mu N_\mu)d\rho^2 + 2N_\mu d\rho dx^\mu + g_{\mu\nu}dx^\mu dx^\nu \tag{4.21}$$

where Greek indices run over $1, ..., D-1$ and are raised and lowered with $g_{\mu\nu}$. The separated coordinate ρ will be related to the radial direction of the black hole. It is important to state the dependence on D of each term at leading order. Note that tis ADM like ansatz separates the radial direction from the beginning, leading to a deeply different split from that in the previous membrane theory ansatz.

Consider a smooth D independent function. The effect of the large D limit will be the infinite growing of the slope of the gradient along its radial direction, since all geometrical effects are localized in a $\sim 1/D$ length scale region. Then we will have, for its radial directional derivative, $\frac{df}{ds_\rho} = \frac{1}{N}\frac{\partial f}{\partial \rho} \sim D$. Recalling this effect holds for D independent functions, we have $\frac{\partial f}{\partial \rho} \sim 1$, so $N \sim 1/D$. A parallel reasoning may be applied to the other radial related quantities in the metric, hence $N^\mu \sim 1/D$. As stated previously, Einstein equations will consist on one scalar, one vector and one tensor equation, after computing the Ricci tensor in 4.21. In vacuum and without

a cosmological constant, Einstein equations are[12]:

$$\frac{1}{N}\partial_\rho K^\mu_\nu + K K^\mu_\nu = R^\mu_\nu - \frac{1}{N}\nabla^\mu\nabla_\nu N + \frac{1}{N}\pounds_N K^\mu_\nu \tag{4.22}$$

$$\nabla_\mu K^\mu_\nu = \nabla_\nu K \tag{4.23}$$

$$K^2 - K_{\mu\nu}K^{\mu\nu} = R \tag{4.24}$$

where all tensors, covariant and Lie derivatives are referred to the $D-1$ submanifold. Here, though, the extrinsic curvature is defined as

$$K_{\mu\nu} = \frac{1}{N}\left(\frac{1}{2}\partial_\rho g_{\mu\nu} - \nabla_{(\mu}N_{\nu)}\right) \tag{4.25}$$

with a global sign difference from 4.20 due to stripping one spacelike dimension instead of the timelike. K is its trace.

4.3.4 Gauge fixing and radial solutions

Recalling the leading order dependencies of N and N^μ, the large D limit simplifies the trace of 4.22 into a solvable equation for the extrinsic curvature, since it reduces to

$$\partial_\rho K + NK^2 = R \tag{4.26}$$

Since the Ricci scalar on the $D-1$ submanifold does not depend on ρ at leading order, the extrinsic curvature is forced to have the shape $K = R(x)f(\rho)$ and the auxiliar coefficient is forced to be $N(x) = 1/R(x)$. Then the solution may be integrated on ρ:

$$K = \frac{f(\rho)}{N(x)} \Rightarrow f' + f^2 = 1 \Rightarrow K = \frac{n}{r_0(x)}\coth\rho + O(D^0) \tag{4.27}$$

after expressing $N(x) = r_0(x)/n$, where r_0 is a D independent curvature radius of the submanifold and $n = D - p - 3 \sim D$ in the limit. We'll use D indistintively from n since the large D limit is being taken by fixing p and letting $n \to \infty$.

It is only now that we distinguish between the worldvolume and the $SO(n+2)$ symmetric directions4.1: the $D-1$ metric is rewritten as[12]

$$g_{\mu\nu}dx^\mu dx^\nu = -(A - u^i u_i/D)dt^2 - 2\frac{u_i}{D}dx^i dt + g_{ij}dx^i dx^j + R_0^2 e^{\frac{2\phi}{n+1}}d\Omega_{n+1} \tag{4.28}$$

where Latin indices run over $1, ..., p$ and are raised and lowered with δ_{ij}. Before solving it at leading order we again need to discuss the D dependence of each term. We can always choose an appropriate timelike coordinate so that $A \sim D^0$. We may also choose a chart for which at leading order the brane is at rest, so the shift vector will be $u \sim 1/D$. Since quasinormal fluctuations along the brane occur in lapses of distance $\sim 1/\sqrt{D}$, we rescale the spacelike coordinates to the mentioned length, so $g_{ij} \sim 1/D$. Furthermore, we can choose the brane spacelike coordinates to be locally Euclidean, so that $g_{ij} = \frac{r_0^2(x)}{n}\delta_{ij} + O(1/D^2)$, proportional to the local curvature radius[12]. The explicit dependence of the angular terms is already specified, so $\phi \sim D^0$.

Recalling the D dimensional spacetime, we impose it to have asymptotical Eddington-Finkelstein shape[12]. Then, $N^2 = N^\mu N_\mu$, and since $g_{tt} = -A$ at leading order, then $N_\mu N^\mu = -AN^{t2} \to N^t = -\frac{N}{\sqrt{A}}$, $N^i = -\frac{N}{\sqrt{A}}u^i$ by covariance (hence $u^i \sim O(D^0)$) and $N^\mu = 0$ for all the $SO(n+2)$ components, since they don't appear in the E-F metric.

Now, the trace of Einstein equations 4.26 may be solved at leading order. The Ricci scalar for this ansatz is $R = D^2/R_0^2 + O(D)$. Then, using the leading order solution for K found in 4.27, we have $\frac{D^2}{r_0^2(x)} = \frac{D^2}{R_0^2}$, so $r_0(x) = R_0$, constant along the whole brane. From now on, we'll assume $r_0 = R_0 = 1$ by simpicity[12].

4.3.5 Extrinsic curvature

We aim now to solve 4.22 in its angular components, which we will label in Latin capitals. By explicit calculation from the definition in 4.25 for our ansatz 4.28,

recalling $N \neq N(x^I)$ and substituting the Ricci tensor, at leading order we have

$$K^I_J = \partial_\rho \phi \delta^I_J \sim O(D^0) \tag{4.29}$$

$$K = D \coth \rho \sim O(D) \tag{4.30}$$

$$R^I_J = D\delta^I_J \sim O(D) \tag{4.31}$$

Again, only the l.h.s. of 4.22 and the Ricci tensor term survive at leading order, simplifying the equation to the fully solvable

$$\partial^2_\rho \phi + \coth \rho \partial_\rho \phi = 1 \Rightarrow \phi = \log m(x^i) + \log \frac{1}{2}(1 + \cosh \rho) + O(1/D) \tag{4.32}$$

being $m(x)$ an integration function only dependent on the brane worldvolume coordinates.

The next step is a repetition of the latter[12]: solving the remaining components of 4.22 at leading order. It's easier, since for our ansatz 4.28 at leading order $R^i_t \sim R^t_i \sim R^i_t \sim O(D^0)$, so the equation is homogeneous for K^t_t and K^i_t. Hence we have:

$$K^t_t = \frac{D}{\sinh \rho} + O(D^0) \tag{4.33}$$

$$K^i_t = \frac{D}{\sinh \rho} v^i + O(D^0) \tag{4.34}$$

$$\tag{4.35}$$

where the constant D/R_0 is fixed in 4.33 after imposing the asymptotic behaviour $A \to -1$ at $\rho \to \infty$. The leading order D dependence can be obtained by inspecting the definition of the extrinsic curvature 4.25. The integration function in 4.41 is not constrained beyond being $O(D^0)$, so there we carry an extra vector v^i which may still be dependent on the worldvolume coordinates. From 4.25 we can now extract the value of the coefficient $A = -g_{tt}$ at leading order:

$$K^t_t = \frac{D}{2} g^{tt} \partial_\rho g_{tt} = \frac{D}{2} \frac{\partial_\rho A}{A} = \frac{D}{\sinh \rho} \tag{4.36}$$

$$A(\rho) = \tanh^2 \frac{\rho}{2} + O(1/D) \tag{4.37}$$

where the integration function is fixed by its asymptotic behaviour. For the $\{it\}$ component:

$$K^i_t = \frac{D}{2}\left(g^{it}\partial_\rho g_{tt} + g^{ij}\partial_\rho g_{tj}\right) = \frac{D}{2}\left(\frac{u^i\partial_\rho A}{A} - \partial_\rho u^i\right) = \frac{Dv^i}{\sinh\rho} \Rightarrow \tag{4.38}$$

$$\Rightarrow \frac{2v_i}{\sinh\rho} = -\partial_\rho u_i + \frac{u_i}{\sinh\frac{\rho}{2}\cosh\frac{\rho}{2}} \tag{4.39}$$

$$u_i = \frac{v_i}{\cosh^2\frac{\rho}{2}} \tag{4.40}$$

where Latin indices in u_i are raised and lowered with the Kronecker deltas. Note that the final solution carries only a particular solution of the non homogeneous linear equation 4.39. A term proportional to the homogeneous solution, $\propto \tanh^2\frac{\rho}{2}$, doesn't appear because of asymptotic conditions at infinite radius.

We can try to find the remaining components of K^μ_ν. After having calculate the connection coefficients for 4.28, simple inspection on the components K^t_i and K^i_j in the definition 4.25 reveals that, contrary to K^i_t or K^t_t, $K^t_i \sim K^i_j \sim O(D^0)$. For K^t_i, equation 4.22 at leading order is again homogeneous, so the solution is

$$K^t_i = \frac{-v_i}{\sinh\rho} + O(1/D) \tag{4.41}$$

where v_i appears as an integration constant and is set to its value after comparing K^t_i with the already known component K^i_t. For K^i_j, the Ricci tensor R^i_j contains one term at order D, $R^i_j \approx -D\partial_i\partial_j \log m$, hence the r.h.s. of 4.22 doesn't vanish anymore at leading order. The solution, then, is only analytical in the asymptotic behaviour for $\rho \to \infty$, $e^-2\rho \to 0$; then the asymptotic behaviour is achieved with[12]

$$K^i_j = -\partial^i\partial_j \log m + \frac{1}{\sinh\rho}\Big(-v^i v_j + \partial^i v_j + \partial_j v^i + \partial^i\partial_j \log m\Big) \tag{4.42}$$

where the worldvolume function in the $1/\sinh\rho$ term emerges as an integration term when solving the equation and is associated to the form in 4.42 after computing the definition 4.25 and comparing with the other known components.

4.3.6 Higher order correction

We aim to take know the last and most important step in order to reach the effective equations. If we pretend to describe non linear features of the dynamics of the brane,

it is compulsory for us to study beyond the leading order in D. Hence, we'll compute now the first order correction on the value of K. Since $K \sim O(D)$, the correction will be $O(D^0)$. Let's examine term by term on trace of 4.22. The leading order terms were $O(D^2)$, so we'll now explicit terms at order and D to impose equality at higher order. Writing $K \approx DK^{(0)} + K^1$ with $K^{(0)} = \coth \rho$ from 4.27, the $O(D)$ terms will be:

- Left hand side: $\frac{1}{N}\partial_\rho(DK^{(0)} + K^{(1)}) + (DK^{(0)} + K^{(1)})^2 \to 2DK^{(0)}K^{(1)}$.

- Right hand side: $R - \frac{1}{N}\nabla^2 N + \frac{1}{N}N^\mu \partial_\mu K \to DR^{(1)}$

being $R \approx D^2 R^{(0)} + DR^{(1)}$. However, we are interested the asymptotic behaviour in ρ. In this limit (always done after the large D in case of indeterminate expressions), the Ricci scalar at $O(D)$ then takes the expression $R = D(-2\partial^i \partial_i \log m - \partial^i \log m \partial_i \log m - 2\log m$, so the correction in the extrinsic curvature is, finally[12],

$$K^{(1)} = -(\partial^i \partial_i \log m + \frac{1}{2}\partial^i \log m \partial_i \log m + \log m) \tag{4.43}$$

4.3.7 Effective equations

We finally have all the tools to build our effective equations. For the scalar effective equation, taking the t component of equation 4.23 gives the equation

$$\partial_t m + \partial_i (m v^i) = 0 \tag{4.44}$$

which is the standard non relativistic conservation law for $m(x^i, t)$. We have to understand m as the horizon density at each worldvolume point[12], so this equation shows energy conservation over the whole brane horizon. The equation contains partial derivatives because it has been derived for cartesian worldvolume coordinates (recall $g_{ij} \propto \delta_{ij}$, so for a general chart one shall substitute ∂_i with ∇_i, covariant derivatives over the spacelike coordinates of the brane, since the equation is non relativistic.

Aside, let's compute now the spatial components of 4.23 in the asymptotic region for ρ. With our knowledge of each K^μ_ν component, Einstein equations will come out as a motion equation for the effective velocity v^i[12]. At leading order plus first order correction, we will have

$$\partial_t v_i + v^j \partial_j v_i = \partial^j \partial_j v_i + \partial_j \partial_i v^j + (\partial_i v_j + \partial_j v_i)\partial^j \log m + \partial_i \Big(\frac{\partial^j \partial_j m}{m} - \frac{\partial^j m \partial_j m}{2m^2} + \log m \Big) \tag{4.45}$$

The same generalization applies here for substituting partial with covariant derivatives for an arbitrary chart. Together, 4.44 and 4.45 are already the effective equations. Nevertheless, they are more compactly expressed in terms of a new variable

$$p_i = \partial_i m + m v_i \tag{4.46}$$

which has a clear interpretation of effective momentum of the mass distribution over the worldvolume. In terms of p_i, the final form of the effective equations for black brane and probably the most important equations for this Dissertation, is

$$(\partial_t - \nabla^2) m = -\nabla_i p^i \tag{4.47}$$

$$(\partial_t - \nabla^2) p_i = \nabla_i m - \nabla^j \Big(\frac{p_i p_j}{m} \Big) \tag{4.48}$$

where all the non linear dynamics of the black brane is concentrated in the last non linear term of 4.48.

As a final remark, the effective equations can also be interpreted as fluid equations. As already discussed, 4.47 is nothing else but a continuity equation for the effective mass distribution. Moreover, one may rewrite equation 4.45 as

$$\partial_t (m v^i) + \nabla_j (m v^i v^j + \tau^{ij}) = 0 \tag{4.49}$$

being

$$\tau_{ij} = -m\delta_{ij} - 2m\nabla_{(i} v_{j)} - m\nabla_j \nabla_i \log m$$

. Recalling the equation of state for a black brane in the large D limit, $\rho \approx -p$, we see that the first term in τ_{ij} has the form of a pressure contribution, and the second term is a viscosity contribution[13]. Hence, we may interpret 4.49 as a standard fluid motion equation with the additional $\propto v^i v^j$ non linear term that characterises our theory.

Related to the effective magnitudes, one may compute three relevant and very natural integral magnitudes[35]: the effective total mass

$$M(t) = \int d^p x \sqrt{g} m(t,x) \tag{4.50}$$

the effective momentum vector

$$P^i(t) = \int d^p x \sqrt{g} p^i(t,x) \tag{4.51}$$

and the effective angular momentum tensor

$$J^{ij}(t) = \int d^p x \sqrt{g} (x^i p^j(t,x) - x^j p^i(t,x)) \tag{4.52}$$

where g is the determinant of the worldvolume metric, which includes all the space dimensions of the brane but excludes time, since the effective theory is fully non relativistic.

The effective equations can also be derived with the help of computational symbolic calculations from the metric

$$ds^2 = -\Big(1-\frac{m(x,t)}{r^n}\Big)dt^2+2dtdr+r^2 d\Omega_{n+1}-\frac{2}{n}\frac{p_i(x,t)}{r^n}dx^i dt+\frac{1}{n}\Big(\delta_{ij}+\frac{1}{n}\frac{p_i(x,t)p_j(x,t)}{r^n m(x,t)}\Big)dx^i dx^j \tag{4.53}$$

Expressing m and p_i as a power series in $1/n$, solving Einstein up to the first higher order will directly recover the effective equations 4.47 and 4.48. From this metric we get an even better intuitive notion of $m(x,t)$ acting as the worldvolume mass density and p_i its worldvolume momentum.

Chapter 5

Applications

In this final chapter we provide several applications of the effective theory for black brane dynamics that has been developed previously. Hence, all our results will emerge from solving the effective equations, 4.47 and 4.48. Several results are obtained with numerical analysis, which we have replicated here for confirmation and clarity using the NDSolve module from Mathematica through self developed codes than can be found in the Appendices.

5.1 Black holes as blobs on the membrane

One may ask how an effective theory entirely developed on a black brane spacetime can provide further understanding of black holes. We prove now that the effective equations 4.47, 4.48 contain different solutions all of the form of localised "blobs" on the mass density field $m(t, x^i)$ that ultimately satisfy all the properties of each type of black holes we've been talking about previously.

5.1.1 Gaussian solutions

Let's consider the simpler scenario of $p = 2$, the simplest brane aside from the black string. We want first to find time independent axisymmetric solutions. We shall, hence, use flat polar coordinates $ds^2 = -dt^2 + dr^2 + r^2 d\phi^2$ on the brane. After a bit of algebra, the effective equations become

$$\Big(\partial_t - \partial_r^2 - \frac{1}{r^2}\partial_\phi^2 - \frac{1}{r}\partial_r\Big)m = -\Big(\partial_r + \frac{1}{r}\Big)p_r - \frac{1}{r^2}\partial_\phi p_\phi \tag{5.1}$$

$$\Big(\partial_t - \partial_r^2 - \frac{1}{r^2}\partial_\phi^2 - \frac{1}{r}\partial_r + \frac{1}{r^2}\Big)p_r + \frac{2}{r^3}\partial_\phi p_\phi = \partial_r m - \partial_r\frac{p_r^2}{m} - \frac{1}{r^2}\partial_\phi\frac{p_r p_\phi}{m} + \frac{1}{r^3}\frac{p_\phi^2}{m} - \frac{1}{r^2}\frac{p_r^2}{m} \tag{5.2}$$

$$\Big(\partial_t - \partial_r^2 - \frac{1}{r^2}\partial_\phi^2 + \frac{1}{r}\partial_r\Big)p_\phi - \frac{2}{r}\partial_\phi p_r = \partial_\phi m - \partial_r\frac{p_r p_\phi}{m} - \frac{1}{r^2}\partial_\phi^2\frac{p_\phi^2}{m} - \frac{p_r p_\phi}{rm} \tag{5.3}$$

We want to find an axisymmetric and static solution: hence nothing can depend on t neither ϕ. Under this assumption 5.1 is solved by $p_r = \partial_r m$, which after substitution in 5.3 gives $p_\phi = mr^2\Omega$ being Ω an integration constant. Equation 5.2 then becomes ordinary for $m(r)$[36]:

$$\Big(\frac{d^2}{dr^2} + \frac{1}{r}\frac{d}{dr} + 1\Big)\log m + \frac{1}{2m^2}\Big(\frac{dm}{dr}\Big)^2 = -\frac{\Omega r^2}{2} \tag{5.4}$$

After rewriting

$$\Omega = \frac{a}{1+a^2} \Leftrightarrow a = \frac{1 \pm \sqrt{1-4\Omega^2}}{2\Omega} \tag{5.5}$$

then 5.4 admits a gaussian family of solutions of the form[36]

$$m(r) = m_0 e^{-\frac{r^2}{2(1+a^2)}} \tag{5.6}$$

written in this notation, a is directly related to the axial angular momentum per unit mass: $J = 2aM$, being M, J the effective mass and angular momentum (its only non vanishing component for $p = 2$) of the brane respectively, by explicit calculation in 4.50 and 4.52. By returning to a cartesian coordinate chart, and thanks to Galilean invariance of the system, we can boost and translate the frame and write the gaussian solution in terms of its spatial velocity and initial position

with respect to the new frame:

$$m(x,y,t) = m_0 e^{-\frac{(x_i - x_{0i} - u_i t)(x^i - {x_0}^i - u^i t)}{2(1+a^2)}} \tag{5.7}$$

$$p_i(x,y,t) = m_0 e^{-\frac{(x_i - x_{0i} - u_i t)(x^i - {x_0}^i - u^i t)}{2(1+a^2)}} \left(u_i + \frac{1}{1+a^2}(a\epsilon_{ij} - \delta_{ij})(x^j - {x_0}^j - u^j t)\right) \tag{5.8}$$

being ϵ_{ij} the spatial Levi-Civita tensor.

5.1.2 Equivalence with Myers-Perry black holes

Consider the Myers-Perry metric in D dimensions 2.23 in the particular case of a singly rotating black hole: $a_1 = a > 0$, all others $a_i = 0$. The resulting metric is identical in both even and odd D[10], more easily derivated from 2.22, and is expressed as

$$ds^2 = -\left(1 - \frac{r_0^{D-3}}{r^{D-5}\Sigma}\right)dt^2 + \frac{2a r_0^{D-3}\sin^2\theta}{r^{D-5}\Sigma}dtd\phi + \left(r^2 + a^2 + \frac{a^2 r_0^{D-3}\sin^2\theta}{r^{D-5}\Sigma}\right)\sin^2\theta d\phi^2 + \\ + \frac{\Sigma}{r^2 + a^2 - r_0^{D-3}/r^{D-5}}dr^2 + \Sigma d\theta^2 + r^2\cos^2\theta d\Omega_{D-4} \tag{5.9}$$

being $\Sigma = r^2 + a^2\cos^2\theta$ as in the standard notation of Kerr metric, and $\mu_1 = \sin\theta$.

Applying now the coordinate change $\rho = r\cos\theta$, followingly replacing $r \to r\sqrt{(D-5)(r^2+a^2)}\sin\theta$ and labeling $R = (1+a^2)\rho^{D-5}$, then the metric 5.9 is rewritten as[36]

$$ds^2 \approx -Adt^2 + \frac{1}{D-5}\frac{2a}{1+a^2}\frac{r^2 e^{-\frac{r^2}{2(1+a^2)}}}{R}dtd\phi + \frac{r^2}{D-5}\left(1 + \frac{r^2}{D-5}\frac{a^2}{(1+a^2)^2}\frac{e^{-\frac{r^2}{2(1+a^2)}}}{R} + \right. \\ \left. + \frac{1}{(D-5)^2}\right)\frac{dR^2}{AR^2} + \frac{1}{D-5}\left(1 + \frac{r^2}{(D-5)(1+a^2)^2}\frac{e^{-\frac{r^2}{2(1+a^2)}}}{AR}\right)dr^2 + \rho^2 d\Omega_{D-4} \tag{5.10}$$

$$A = 1 - \frac{e^{-\frac{r^2}{2(1+a^2)}}}{R}$$

where terms at higher orders in $1/D$ have been omitted. Finally, we just need to redefine two coordinates[36]: $t \to t + \frac{1}{D-5}\log(AR)$ and $\phi \to \phi - \frac{1}{D-5}\frac{a}{1+a^2}\log(AR)$.

Then, the previous metric 5.10 has exactly the form of 4.53 as long as we identify

$$m(r) = e^{-\frac{r^2}{2(1+a^2)}} \tag{5.11}$$

$$p_r(r) = -\frac{r}{1+a^2} e^{-\frac{r^2}{2(1+a^2)}} \tag{5.12}$$

$$p_\phi(r) = \frac{ar^2}{1+a^2} e^{-\frac{r^2}{2(1+a^2)}} \tag{5.13}$$

which are exactly the expressions of the effective mass and momenta for the gaussian blob solution as defined in 5.6. Hence, we have proved that gaussian blob solutions with spin a may be perfectly interpreted as single spinning Myers-Perry black holes in the large D limit.

5.1.3 Quasinormal modes

We will now extract the quasinormal spectrum of the slow modes in the Schwarzschild-Tangherlini particular case, i.e. $a = 0$, since we discussed it in previous chapters. Consider the non spinning case of 5.6 and consider an infinitesimal periodic perturbation:

$$\delta m(t, r, \phi) = \delta_m(r) e^{-i\omega t + i m_\phi \phi} \tag{5.14}$$

$$\delta p_r(t, r, \phi) = \delta_r(r) e^{-i\omega t + i m_\phi \phi} \tag{5.15}$$

$$\delta p_\phi(t, r, \phi) = \delta_\phi(r) e^{-i\omega t + i m_\phi \phi} \tag{5.16}$$

where all $\delta_i << 1$. Effective equations at linear order on the perturbations will establish relations between the radial functions δ_i. In concrete, on can prove [36] that a combination of them lead to

$$\prod_{i=1}^{3} \left[\frac{d^2}{dr^2} \left(\frac{1}{r} - r \right) \frac{d}{dr} + m_\phi + 2k_i - \frac{m_\phi^2}{r^2} \right] \frac{\delta_m}{m} = 0 \tag{5.17}$$

where k_i are the three solutions of a cubic equation,

$$k^3 - \frac{\gamma}{2} k^2 + \frac{\gamma(1+\gamma) - 6 + 3m\phi}{12} k - \frac{(\gamma+3)(9m\phi - 9 + \gamma^2)}{216} = 0 \tag{5.18}$$

which is, itself, dependent on the frequency ω via $\gamma = 3(1 + i\omega - m_\phi)$. Nevertheless, equation 5.17 only is regular at both $r = 0$ and asymptotic infinity under the condition on k_i to be natural[36], in which case the solutions are Laguerre polynomials.

Using $\ell = 2k - m_\phi$ (obviously m_ϕ must be integer by continuity of the perturbation), the imposition of k being natural (hence ℓ being integer) gives in return the quantisation condition of the frequency spectrum, which is nothing else than rewriting 5.18 in terms of ℓ and finding the solutions for ω:

$$\omega^3 - i(4-3\ell)\omega^2 - (\ell-1)(3\ell-4)\omega - i\ell(\ell-2)(\ell-1) = 0 \tag{5.19}$$

which has, of course, three complex solutions for ω, only one being real:

$$\omega_\pm = -i(\ell-1) \pm \sqrt{\ell-1}, \quad \omega_0 = -i(\ell-2) \tag{5.20}$$

The purely imaginary frequency corresponds to a stationary mode (non periodic) that exponentially decays with time. The frequencies $\omega_\pm$ are exactly of the form of 3.48, the scalar modes, up to order at leading order for large D, while ω_0 is exactly the leading order of 3.47, the vector modes, after a unit shift in ℓ due to different definitions. Note that since $Im\omega < 0$ for all the mentioned modes, by inspection in equations 5.14, 5.15 and 5.16, then the three of the modes are stable since their module decays with time. Of course, the spectrum we've found corresponds to the decoupled QNM, since only they are localised on the near zone of the black hole and, hence, can be described with an effective theory.

More general and vastly longer calculations may be done in the general Myers-Perry case $a \neq 0$ to end up obtaining the quasinormal spectrum of Myers-Perry black holes[19, 36], which is a direct (and necessary!) consequence of being able to interpret axisymmetric stationary black holes as gaussian blobs on a brane in our effective theory.

5.1.4 Black bars

Effective equations also contain a solution that, though no longer axisymmetric, has great physical importance for the following sections: the *black bar* solution (still considering a 2-brane)[35], in which the the effective density takes the following expression:

$$m(t,r,\phi) = m_0 e^{\left[1-\frac{r^2}{4}\left(1-\sqrt{1-4\Omega^2}\cos[2(\phi-\Omega t)]\right)\right]} \tag{5.21}$$

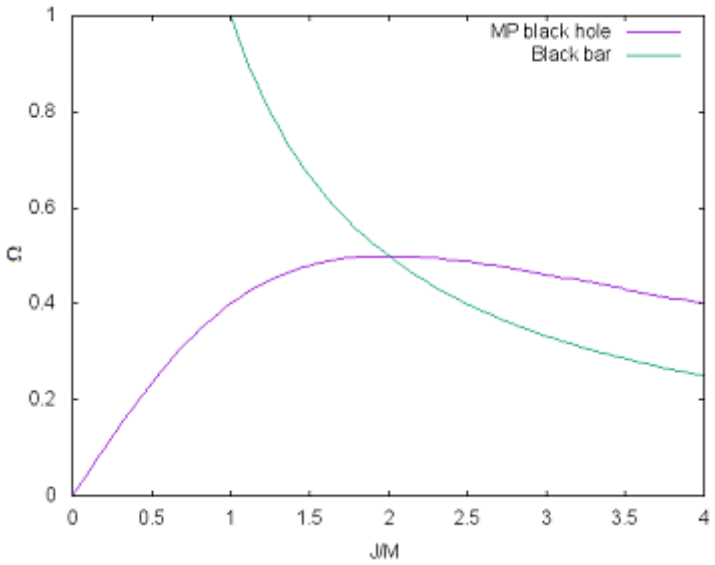

Figure 5.1: This simple graphic illustrates the very different dependence between Ω and J/M for Myers-Perry black holes and black bars. Their functions intersect at $J/M = 2$ with $\Omega = 1/2$, which in addition is its critical value and upper bound for a black bar.

The shape of 5.21 is actually that of a rotating bar with constant angular velocity Ω. The bar behaviour is intuitive: given a concrete direction from the origin, i.e. for an arbitrary value of ϕ, m will be a gaussian blob oscillating in width with time over a period of $2\pi/\Omega$, and the term with a cosine will determine the maximum and minimum width the bar may take, i.e. its longitudinal and transverse lengths, respectively. Since a gaussian distribution takes the form of $\sim e^{-x^2/(2\sigma^2)}$ being σ its standard deviation, we can identify the characteristic length scale of a gaussian blob as its standard deviation. Hence, by inspection and comparison, the longitudinal and transverse lengths corresponding to the maximum and minimum deviation will be

$$\ell_L^2 = \frac{2}{1-\sqrt{1-4\Omega^2}}, \quad \ell_T^2 = \frac{2}{1+\sqrt{1-4\Omega^2}} \tag{5.22}$$

By explicit integration through their definitions, one can check that $\Omega^{-1} = J/M$. Hence, angular momentum per unit mass is no longer proportional to the rotating frequency as one would naively expect, but proportional to its inverse. Note that the solution only exists for $\Omega \in [-1/2, +1/2]$ and the critical value $\Omega = \pm 1/2$

recovers axisymmetry: in fact, it is the exact solution of a singly spinning Myers-Perry black hole as a gaussian blob 5.6 taking $a = 1$. Furthermore, note how the angular momentum of unit mass, due to the restriction on the values of Ω, presents a lower bound so that $J/M \geq 2$ (see 5.1): infinitely slow black bars do not exist.

5.2 Black hole collisions

The black hole interpretation of gaussian blobs on the brane enables us to study black hole phenomenology in the large D limit using our effective theory for black branes. We'll start by analysing collisions between two black holes. This must be computed numerically.

5.2.1 Initial configuration

Our initial configuration will be two Myers-Perry black holes with equal or opposite spin by simplicity and located far away from each other. Hence, the initial configuration of the mass distribution m can be approximated as the direct sum of two gaussian blobs 5.7 located around different points (x_0, y_0) with relative velocity that makes them get closer with time. The direct sum approximation will be also valid for building the initial configurations of p_i. We can always choose a cartesian 2-dimensional chart so that the center of mass is at rest and set to the origin, and align the relative velocity, say, to the x axis, following the same choices as [35]. Then, the initial system will the depend on five parameters: x_0, $y_0 = \pm b/2$, u, a and m_0, the mass at the center of the blob which we require it to be equal for both blobs. Under these assumptions, the initial configuration will be (see figure 5.2)

$$m = m(m_0, -x_0, -b/2, +u, 0, a) + m(m_0, +x_0, +b/2, -u, 0, \pm a) \tag{5.23}$$

where $m(m_0, x_0, y_0, u_x, u_y, a)$ are the isolated gaussian blobs 5.7 with particular values on the parameters.

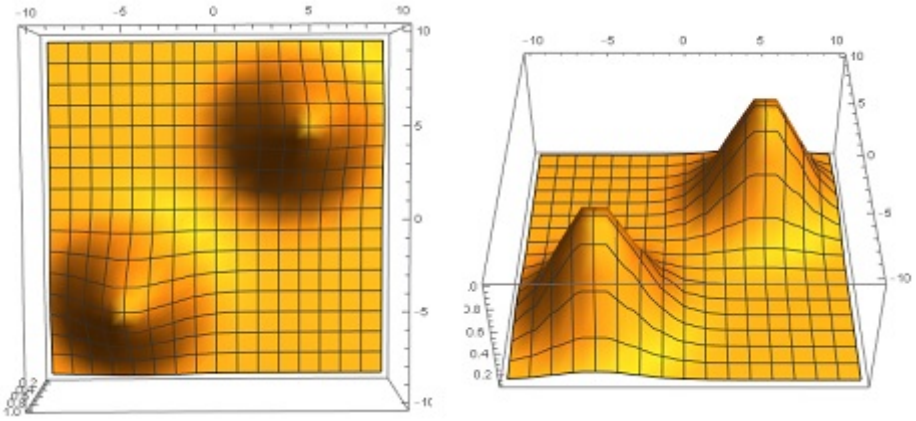

Figure 5.2: Plot of the discussed initial state of $m(x, y)$ with arbitrary parameters $x_0 = 5$, $b = 10$, $m_0 = 1$, $a = 2$ and $u = 3$.

To numerically run the effective equations, we further need boundary conditions for the worldvolume coordinates domain. Simply, by working in a square of length $L >> x_0 \sim b$, one can require Dirichlet homogeneous conditions and the boundary without any inconvenience. By consistency, we set m, p_i to be very small constants at the boundaries but not exactly zero to avoid numerical divergences: recall 4.48 contains a dividing m in the non linear term, so non of the effective functions can vanish completely. It has been computed that collisions at large relative velocity u results in the formation of ≥ 2 objects. We'll therefore always use small velocities to that a $2 \to 1$ or $2 \to 2$ scattering is guaranteed.

5.2.2 Numerical Results

Here we'll discuss the results achieved in [35] and we will illustrate them with some examples taken from our own numerical simulations, using the NDSolve module to numerically solve PDE systems in Mathematica.

The results show both qualitative and quantitative interesting features. On one hand, one could ask what objects and how many of them should we expect in the final state and, if they exist, in intermediate states. As consequence, of course, we'd want to know the values of our parameter set for which these features are modified, and to finally draw some kind of phase diagram for black hole collision.

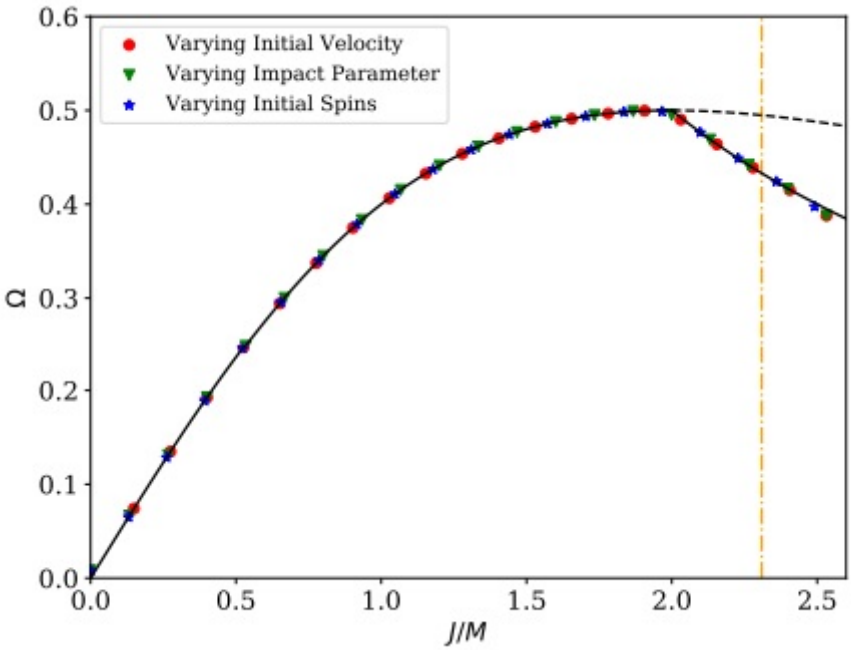

Figure 5.3: This figure is taken from [35], representing three numerical sets of simulations varying u (red), b (green) and a (blue), for two parallel spinning black holes. The orange line marks the upper limit of black bar stability at longer time scales.

The first fundamental result is that the final resulting outcome from our discussed initial configuration exclusively depends on the initial angular momentum, as defined in 4.52. This can be proved by running several sets of simulations varying at each set one single different parameter and plotting the results, for example the angular velocity Ω of the final state if it contains a single object, as a function of the varying angular momentum. One realizes that all sets of data are identical (Figure 5.3). Note that, because of the lack of gravitational radiation emission in the large D limit, total angular momentum is conserved throughout the evolution in all the simulations[37].

The shape of 5.3 also replicates figure 5.1 and, for $J/M > 2$, we see that numerical simulations predict a black bar type final state over a Myers-Perry black hole. Hence, for $J/M > 2$ Myers-Perry black holes are unstable. Eventually, black bars become unstable too for $J/M = 4/\sqrt{3}$ (the value of the orange dashed line in 5.3). As a brief justification, when Ω keeps decreasing the longitudinal and transverse lengths 5.22 diverge and vanish respectively, so the black bar approaches the configuration of a

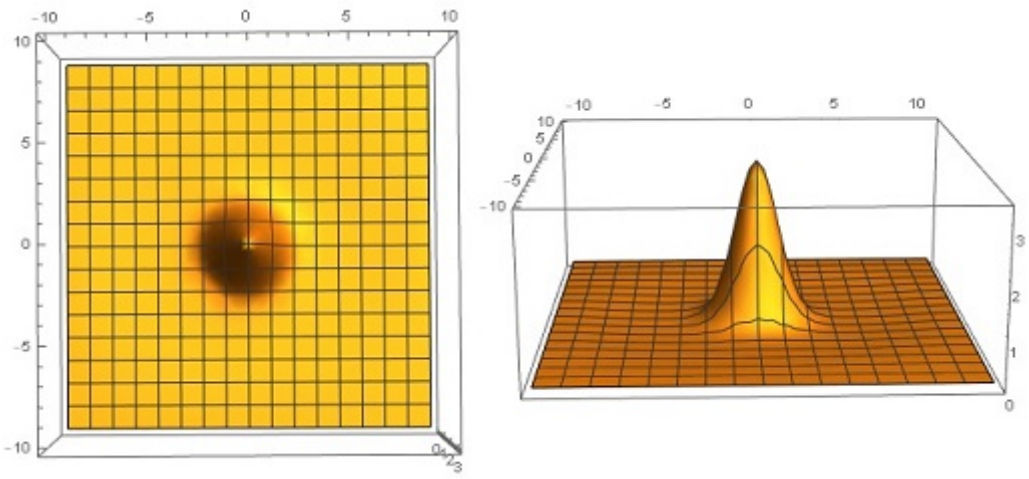

Figure 5.4: Graphic plot of the final state of $m(x, y)$ for $u = 1.7$, $a = 0$ and $b = 1$. We clearly see that the final object is a perfectly round gaussian blob, i.e. a Myers-Perry black hole. Note that despite having two Schwarzchild-Tangherlini black holes initially, as $a = 0$, the final state must be Myers-Perry due to a total non vanishing angular momentum caused by the impact parameter $b \neq 0$.

black string. Then $J/M = 4/\sqrt{3}$ corresponds to its first unstable mode[35] related to the black string Gregory-Laflamme instability.

The two following figures 5.4 and 5.5 are the result of two example cases after numerically computing the effective equations by ourselves. We can check that the results match with those from published papers.

5.2.3 Violation of Cosmic Censorship

Up until now, all the results that have been discussed were computed with a reasonably low total angular momentum per unit mass in the initial configuration. Thanks to this restriction, all the final outcomes consisted in one single object, either a M-P black hole or a black bar. One may ask what happens if we keep increasing the total angular momentum, were both M-P black holes and black bars are unstable.

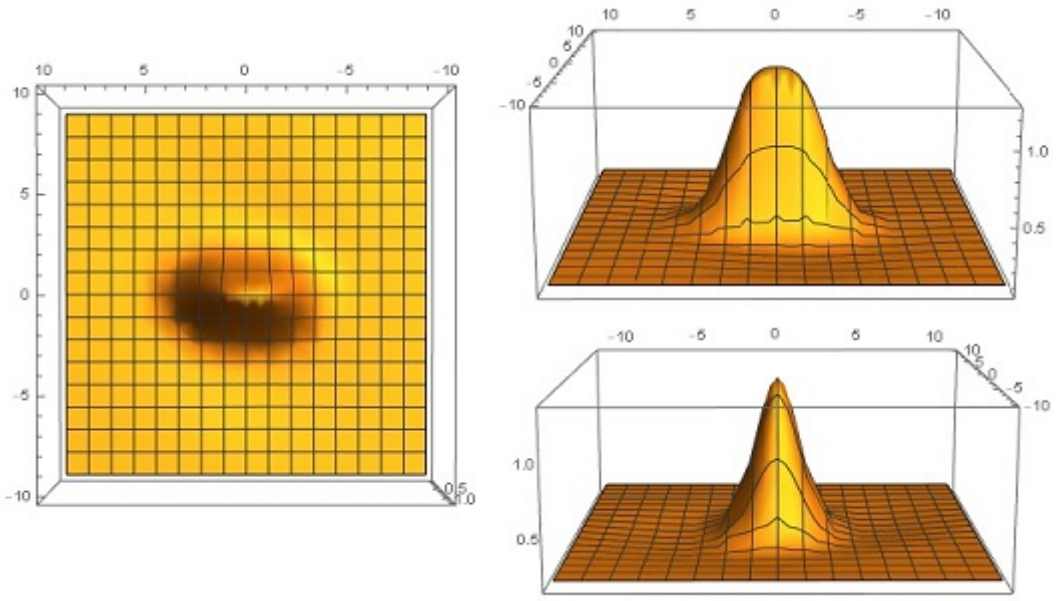

Figure 5.5: Graphic plot of the final state of $m(x, y)$ for $u = 1.7$, $a = 0$ and $b = 2.5$. We clearly see that the final object is no longer a circular blob but a distribution with two orthogonal main axis: it is a black bar. Further figures over a small time interval would show how the bar rotates.

Hence, we now run again simulations with two initial gaussian blobs but using a set of parameters u, a and b so that J/M is larger that the threshold for black bar stability: $J/M > 4/\sqrt{3} \approx 2.31$. For J/M slightly greater than the critical value, the final state still contains a black bar. This is due to the long time scale of the black bar instability when J/M is close enough to the threshold.

One needs to reach an angular momentum $J/M > 2.43$[37, 35] if, like in our simulations, we run $t \in [0, 10]$. When we run the equations under these conditions, the result we obtain is an intermediate short lived black bar due to Gregory-Laflamme type instabilities followed by a smooth split through its middle section and, eventually, a complete separation into two independent Myers-Perry gaussian blobs, in general different from the incoming black holes (see figure 5.6.

The physical relevance of the black bar split is deeper that what it seems on the surface since. The fact of the horizon density of the black decaying into zero implies,

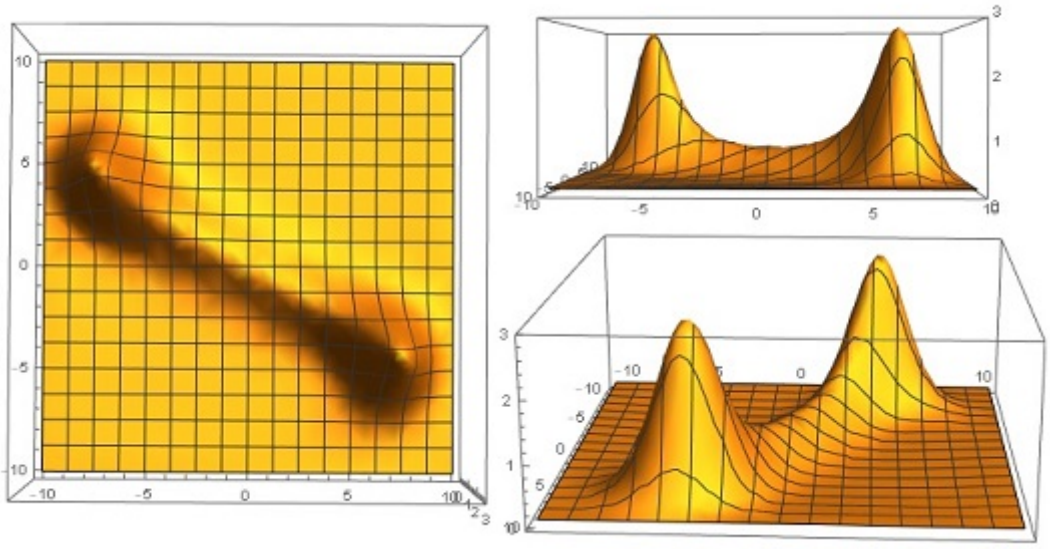

Figure 5.6: These figures show the shape of $m(x, y)$ at $t = 5$ with an initial configuration with $u = b = x_0 = 3$ and $a = 2$ with parallel spinning black holes. With these parameters, the angular momentum satisfies $J/M > 2.43$ and, as expected, the black bar ends up splitting into two black holes.

remarkably, a violation of Cosmic Censorship[37, 35, 38]. Weak Cosmic Censorship is a conjecture which, roughly, states that all curvature singularities that arise from gravitational collapse must be hidden within a black hole[2]. Consequently, Cosmic Censorship (CC) forbids the existence of naked curvature singularities. Hence, CC would forbid the horizon of the black bar to completely shrink to zero in its center, where the singularity remains. We can never see it explicitly through an effective theory (since the horizon density is never exactly zero), since a perturbative expansion in $1/D$ no longer well defined around a singularity; we would need curvatures smaller than $1/D$[37]. However, the result matches with other studies [38], and its natural interpretation itself suggest a complete shrink of the horizon at the origin, violating CC.

This result through the effective theory is one more prove that suggests that Cosmic Censorship may be violated in spacetimes with dimension higher than $D = 4$[38, 37].

5.3 The black string instability

5.3.1 Equations and initial state

As we have explained in previous chapters, at $D \geq 5$ and lower than some higher value around $D \approx 13$, black branes are Gregory-Laflamme unstable[7]. Here, we'll try to show this instability in a numerical simulation of the effective equations for a black string and, furthermore, investigate the final state of this instability and give some interpretation of it. Hence, throughout this section we'll be following [39] with our own simulations as a confirmation of the results.

For a black string the effective equations are simple: from 4.47 and 4.48, the black string equations will be

$$(\partial_t - \partial_z^2) m(t,z) = -\partial_z p(t,z) \tag{5.24}$$

$$(\partial_t - \partial_z^2) p(t,z) = \partial_z \Big(m(t,z) - \frac{p(t,z)^2}{m(t,z)} \Big) \tag{5.25}$$

We assume the string is compactified, i.e. the solution is periodic in z. So, we can simply restrict $z \in [-L/2, +L/2]$, so that the solution will have an associated wavenumber $k = 2\pi/L$.

For the initial state, we will take a perturbation from the static uniform string:

$$m(0,z) = 1 + \delta_m(z), \quad p(0,z) = \delta_p(z) \tag{5.26}$$

so that the center of mass is at rest and located at the origin, i.e. $P = 0$ as defined in 4.51. We can start the simulation with, say, a periodic perturbation (see figure 5.7)

$$\delta_m(z) = \epsilon \cos(kz), \quad \delta_p(z) = \frac{d}{dz}\delta_m(z) = -\frac{1}{k}\epsilon \sin(kz) \tag{5.27}$$

with $\epsilon << 1$. Since the perturbation is even in z, periodic boundary conditions in $\pm L/2$ will reduce to homogeneous Neumann conditions for the $m(t, \pm L/2)$ and Dirichlet conditions for $p(t, \pm L/2)$.

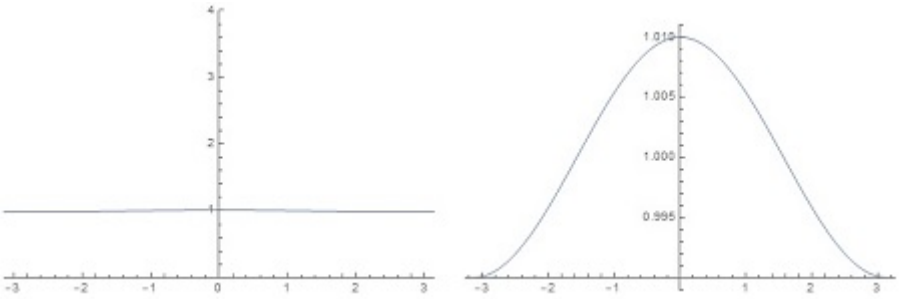

Figure 5.7: Initial profile of the mass density $m(z)$. On the right, a zoom in of the left graphic to appreciate the shape of the initial perturbation. We'll always use $\epsilon = 0.01$ and, here, $L = 1$ arbitrarily.

5.3.2 Numerical results

The final outcome can be summarized in the following features:

- Final shape: For all values of k between $1/2$ and 1, the final state is a non uniform black string with one single blob centered at $z = 0$ whose peak decreases with k (see figures 5.8 and 5.9), since it can be reasonably well approximated to gaussian, $m \sim Le^{-z^2/2}$, regardless of the initial shape of the perturbation. For values of k below the previous range, i.e. longer strings, the final state depends on out initial choice for $\delta_m(z)$ and may end un showing more than one blob. For $k > 1$, instead, the perturbation is stable and the string quickly returns to the uniform configuration[39] (see figure 5.7).

- Time scale: For the most relevant range $1/2 < k < 1$, we see that the equilibrium final state, i.e. the endpoint, is reached faster as k decreases. This is a general feature; however, the total time spent may still depend on the initial shape of the perturbation.

Hence, our effective theory predicts that the endpoint of unstable compactified black strings will be non uniform black strings, whose shape and evolution time will depend on length.

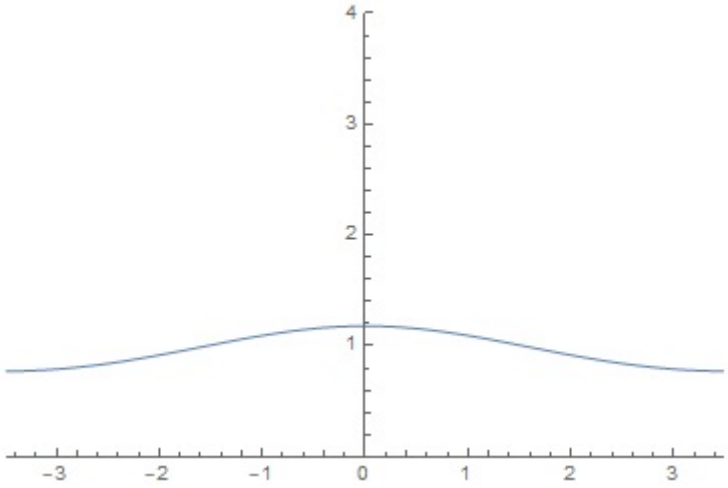

Figure 5.8: Final outcome of the perturbed black string at $t = 25$ for $k = 0.9 \in (0.5, 1)$. We see that the infinitesimal perturbation grows into a moderately non uniform black string with a peak at $m \approx 1.2$.

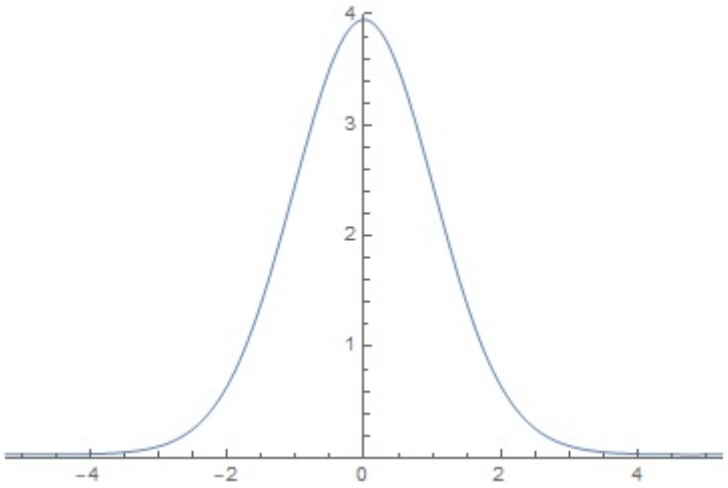

Figure 5.9: Final outcome of the perturbed black string at $t = 25$ for $k = 0.6 \in (0.5, 1)$. We see that the infinitesimal perturbation grows into a sharply non uniform black string with a peak at $m \approx 4.0$, much higher than the peak for higher values of k. We also see that the mass density in the extremes tends to zero quicker than in the other cases.

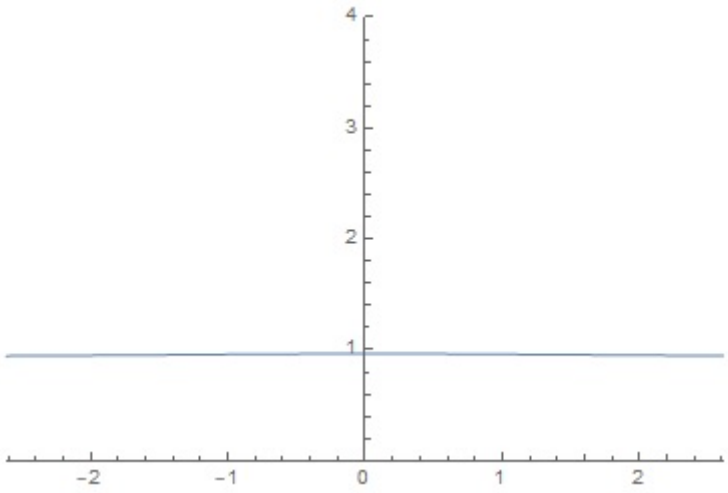

Figure 5.10: Final outcome of the perturbed black string at $t = 25$ for $k = 1.2 > 1$. We see that the perturbation hasn't grown and the string remains uniform. Hence, the uniform string is stable.

Chapter 6

Conclusion

As a conclusion for this Dissertation, here we review and summarize the main results of the project.

In chapter 2 we've seen than General Relativity is naturally extendable to a higher number of space dimensions. In concrete, the generalization of black hole solutions in vacuum expands to a great spectrum of geometries: some of them are straight generalizations from $D = 4$ cases, such as the Schwarzschild-Tangherlini solution for spherically symmetric and static black holes and the Myers-Perry solutions for stationary rotating black holes. Other geometries such as brack strings, black branes or black rings are completely novel. Uniquess theorems, hence, no longer hold. The study of black hole dynamics in higher D gets drastically simplified using the large D limit, which implies working at leading and first higher order in $1/D$ in all objects. For a black hole, the large D limit restricts all gravitational effects into a thin layer of width r_0/D around the event horizon, leaving the outer spacetime flat at leading order

In chapter 3 we have found how, at any D, perturbative dynamics of black holes are described in terms of *quasinormal modes*, which are harmonic eigenfunctions that transform as scalars, vectors or tensors in the maximally symmetric submanifold. Given the absorptive nature of the black hole, their frequencies are not necessarily

real, bringing the possibility of quickly dissipative or unstable modes. The allowed frequencies may be quantised due to asymptotic and horizon boundary conditions. In the large D limit, the frequency spectrum of quasinormal modes of black holes can be disjointedly classified into universal fast non decoupled modes, with frequencies proportional to D without extra information, and slow decoupled modes with frequencies independent of D at leading order, localised around the horizon and with rich physical information that makes them unique of each solution.

In chapter 4 we've followed the derivations where, for appropriate ansatzs, solving Einstein equations up to the first higher order in $1/D$ gives rise to sets of effective equations that operate on effective variables in terms of which non linear dynamics of large D black branes can be described by means of an effective theory.

Finally, in chapter 5 we have studies how static gaussian type solutions of the black brane effective equations may be interpreted as singly spinning Myers-Perry black holes, making the effective theory of black branes able to describe dynamical features such as collisions or fluctuations.

Regarding black hole collision we have confirmed that, depending only on the total initial angular momentum per unit mass J/M, collisions between two singly spinning Myers-Perry black holes evolve into a final single M-P black hole for low J/M, a rotating black bar solution for higher J/M and, ultimately for even higher J/M, a break out of the bar into two new and separate M-P black holes, violating Cosmic Censorship in the process.

In parallel, due to the Gregory-Laflamme instability, we have checked that initially uniform compactified black strings with an infinitesimal perturbation may have different endpoints depending on its compactified length. For short strings the perturbation is stable and quickly vanishes. For longer lengths, the perturbation grows into a final stable state where the black ring is no longer uniform, being the deformation larger and faster to reach equilibrium as the length of the string grows.

These are only two applications of one of the two effective theories in the large D limit that have been studied here. Other problems may be dealt using the mentioned tools such as the stability of ultraspinning Myers-Perry black holes[40] or the quasi-normal spectrum of rotating black holes[19]. Hence, we end up this Dissertation by acknowledging one last time how the classical study of black holes, in concrete their study in the large D limit, has still a lot of topics to continue researching at, hence being arguably a hot field in current physics investigation.

Appendix A

Black hole collision code

```
u = 3
x0 = 5
b = 10
a = 2
M = 1
m1[x_, y_] = M * Exp[-((x + x0)^2 + (y + b / 2)^2) / (2 * (1 + a^2))]
                exponencial
m2[x_, y_] = M * Exp[-((x - x0)^2 + (y - b / 2)^2) / (2 * (1 + a^2))]
                exponencial
m0[x_, y_] = 0.1 + m1[x, y] + m2[x, y]
p1x[x_, y_] = D[m1[x, y], x] + m1[x, y] * (u + a * b / (2 * (1 + a^2)))
                deriva
p2x[x_, y_] = D[m2[x, y], x] + m2[x, y] * (-u - a * b / (2 * (1 + a^2)))
                deriva
p1y[x_, y_] = D[m1[x, y], y] - m1[x, y] * a * x0 / (1 + a^2)
                deriva
p2y[x_, y_] = D[m2[x, y], y] + m2[x, y] * a * x0 / (1 + a^2)
                deriva
p0x[x_, y_] = p1x[x, y] + p2x[x, y]
p0y[x_, y_] = p1y[x, y] + p2y[x, y]

mb1 = m0[-10, y]

mb2 = m0[+10, y]

mb3 = m0[x, -10]

mb4 = m0[x, +10]
```

```
pbx1 = p0x[-10, y]

pbx2 = p0x[+10, y]

pbx3 = p0x[x, -10]

pbx4 = p0x[x, +10]

pby1 = p0y[-10, y]

pby2 = p0y[+10, y]

pby3 = p0y[x, -10]

pby4 = p0y[x, +10]

sol =
 NDSolve[{D[m[t, x, y], t] - Laplacian[m[t, x, y], {x, y}] ==
 |resolvedo··· |deriva                |laplaciano
     -Div[{px[t, x, y], py[t, x, y]}, {x, y}],
      |divergencia
D[px[t, x, y], t] - Laplacian[px[t, x, y], {x, y}] ==
|deriva               |laplaciano
    D[m[t, x, y], x] -
    |deriva
     Div[{px[t, x, y] px[t, x, y] / m[t, x, y],
     |divergencia
       px[t, x, y] py[t, x, y] / m[t, x, y]}, {x, y}],
D[py[t, x, y], t] - Laplacian[py[t, x, y], {x, y}] ==
|deriva               |laplaciano
    D[m[t, x, y], y] -
    |deriva
     Div[{py[t, x, y] px[t, x, y] / m[t, x, y],
     |divergencia
       py[t, x, y] py[t, x, y] / m[t, x, y]}, {x, y}],
m[0, x, y] == m0[x, y], px[0, x, y] == p0x[x, y], py[0, x, y] == p0y[x, y],
   m[t, -10, y] == mb1, m[t, +10, y] == mb2, m[t, x, -10] == mb3,
   m[t, x, +10] == mb4,
px[t, -10, y] == pbx1, px[t, +10, y] == pbx2, px[t, x, -10] == pbx3,
   px[t, x, +10] == pbx4, py[t, -10, y] == pby1, py[t, +10, y] == pby2,
   py[t, x, -10] == pby3, py[t, x, +10] == pby4},
{m, px, py}, {t, 0, 10}, {x, -10, +10}, {y, -10, +10}]

Plot3D[m[0., x, y] /. sol, {x, -10, 10}, {y, -10, 10}, PlotRange → All]
|representación gráfica 3D                                |rango de rep··· |todo
```

Appendix B

Black string instability code

```
eps = 0.01;

m0[z_] = 1. + eps * Cos[k * z]
                    coseno

p0[z_] = D[m0[z], z]
          deriva

k = 0.6
L = 2 Pi / k;
      número

sol =
 NDSolve[{D[m[t, z], t] - D[m[t, z], {z, 2}] == -D[p[t, z], z],
  resolvedo···  deriva          deriva                 deriva

D[p[t, z], t] - D[p[t, z], {z, 2}] ==
deriva          deriva

      D[m[t, z], z] - D[p[t, z] * p[t, z] / m[t, z], z],
       deriva          deriva

m[0, z] == m0[z], p[0, z] == p0[z], m^(0,1)[t, -L / 2] == 0,
    m^(0,1)[t, L / 2] == 0, p[t, -L / 2] == 0, p[t, L / 2] == 0},
{m, p}, {t, 0, 25}, {z, -L / 2, L / 2}][[1]]

tval = 25.;

Plot[m[tval, z] /. sol, {z, -L / 2, L / 2},
representación gráfica
 PlotRange → {{-L / 2, +L / 2}, {0, 4}}]
 rango de representación

Plot[p[tval, z] /. sol, {z, -L / 2, L / 2},
representación gráfica
 PlotRange → {{-L / 2, +L / 2}, {0, 4}}]
 rango de representación
```

Bibliography

[1] Pawel O. Mazur. Black Uniqueness Theorems. 2000.

[2] Robert M. Wald. Gravitational collapse and cosmic censorship, 1997.

[3] Roberto Emparan and Harvey S. Reall. Black Holes in Higher Dimensions. 2008.

[4] Veronika E. Hubeny. The AdS/CFT correspondence. 2014.

[5] Roberto Emparan and Christopher P. Herzog. The large D limit of Einstein's equations, 2020.

[6] Roberto Emparan, Ryotaku Suzuki, and Kentaro Tanabe. The large D limit of General Relativity. 2013.

[7] R. Gregory and R. Laflamme. Black strings and p-branes are unstable. 1993.

[8] F. R. Tangherlini. Schwarzschild field in n dimensions and the dimensionality of space problem. *Il Nuovo Cimento*, 27(3), 2 1963.

[9] K. Schwarzschild. On the gravitational field of a mass point according to einstein's theory. 1999.

[10] Robert C. Myers. Myers-Perry black holes, 2011.

[11] Robert C. Myers. Stress tensors and Casimir energies in the AdS/CFT correspondence. 1999.

[12] Roberto Emparan, Keisuke Izumi, Raimon Luna, Ryotaku Suzuki, and Kentaro Tanabe. Hydro-elastic complementarity in black branes at large d. 2016.

[13] Eric Gourgoulhon. An introduction to relativistic hydrodynamics. 2006.

[14] A. N. Aliev. Rotating black holes in higher dimensional einstein-maxwell gravity. 2006.

[15] Jutta Kunz, Dieter Maison, Francisco Navarro-Lerida, and Jan Viebahn. Rotating einstein-maxwell-dilaton black holes in d dimensions. 2006.

[16] M. Socolovsky. Schwarzschild black hole in Anti-de Sitter space, 2017.

[17] Roberto Emparan and Harvey S. Reall. Black rings. 2006.

[18] Kentaro Tanabe. Black rings at large D. 2015.

[19] Oscar J. C. Dias, Gavin S. Hartnett, and Jorge E. Santos. Quasinormal modes of asymptotically flat rotating black holes. 2014.

[20] Roberto Emparan, Ryotaku Suzuki, and Kentaro Tanabe. Decoupling and non-decoupling dynamics of large D black holes. 2014.

[21] Hideo Kodama, Akihiro Ishibashi, and Osamu Seto. Brane world cosmology - gauge-invariant formalism for perturbation. 2000.

[22] Hideo Kodama and Akihiro Ishibashi. A master equation for gravitational perturbations of maximally symmetric black holes in higher dimensions. 2003.

[23] Hideo Kodama and Akihiro Ishibashi. Master equations for perturbations of generalised static black holes with charge in higher dimensions. 2003.

[24] Amruta Sadhu and Vardarajan Suneeta. Schwarzschild-Tangherlini quasinormal modes at large D revisited, 2018.

[25] Roberto Emparan and Kentaro Tanabe. Universal quasinormal modes of large D black holes. 2014.

[26] Ruth Gregory. The Gregory-Laflamme instability, 2011.

[27] Peter-Simon Dieterich, Uwe Semmelmann, and Günter Wunner. *On the Lichnerowicz Laplace operator and its application to stability of spacetimes*. PhD thesis.

[28] Roberto Emparan, Tetsuya Shiromizu, Ryotaku Suzuki, Kentaro Tanabe, and Takahiro Tanaka. Effective theory of black holes in the 1/D expansion, 2015.

[29] Sayantani Bhattacharyya, Anandita De, Shiraz Minwalla, Ravi Mohan, and Arunabha Saha. A membrane paradigm at large D. 2015.

[30] R. Arnowitt, S. Deser, and C. W. Misner. The Dynamics of General Relativity. 2004.

[31] Theodor Kaluza. On the problem of unity in physics.

[32] Oskar Klein. Quantum theory and five-dimensional relativity theory. *The Oskar Klein Memorial Lectures 1988-1999*, 02 2014.

[33] Gary T. Horowitz and Toby Wiseman. General black holes in Kaluza-Klein theory, 2011.

[34] Edmund Bertschinger. Hamiltonian Formulation of General Relativity, 2002.

[35] Tomas Andrade, Roberto Emparan, David Licht, and Raimon Luna. Black hole collisions, instabilities, and cosmic censorship violation at large D. 2019.

[36] Tomas Andrade, Roberto Emparan, and David Licht. Rotating black holes and black bars at large D. 2018.

[37] Tomas Andrade, Roberto Emparan, David Licht, and Raimon Luna. Cosmic censorship violation in black hole collisions in higher dimensions. 2018.

[38] Luis Lehner and Frans Pretorius. Black strings, low viscosity fluids, and violation of Cosmic Censorship. 2010.

[39] Roberto Emparan, Ryotaku Suzuki, and Kentaro Tanabe. Evolution and endpoint of the black string instability: Large D solution. 2015.

[40] Oscar J. C. Dias, Pau Figueras, Ricardo Monteiro, and Jorge E. Santos. Ultraspinning instability of rotating black holes. 2010.